Recent Advances in Functional Nanoparticle Assemblies

Franziska Lübkemann-Warwas, Irene Morales, and Nadja C. Bigall*

Assemblies of colloidal nanoparticles (NPs) into various functional superstructures, such as ordered or nonordered, microscopic or macroscopic, and templated or self-supported, have recently attracted a lot of research interest. The continuous development of colloidal nanoparticle synthesis enables a fine-tuning of the structure and properties of such functional superstructures leading to numerous new applications. Herein, it is aimed to summarize a variety of assemblies based on ordered self-assembled NPs, e.g., stacked nanoplatelets, and nonordered self-assembled NPs, e.g., nanoparticle-based aerogels and cryoaerogels, systems ranging from the microscopic to the macroscopic range. Depending on the materials of the nanoparticle building blocks used, e.g., metallic, magnetic, semiconducting, or their combination in hybrid systems, both ordered and nonordered assemblies yield interesting properties for a wide variety of applications, such as catalysis, photocatalysis, or sensing, which are highlighted and discussed.

1. Introduction

Nowadays, years of research in colloidal synthesis of nanomaterials and the progress made on that behalf allow to produce nanoparticles (NPs) with a huge control over the size, shape, and material composition, e.g., metallic, semiconducting, magnetic, hybrid, or mixed systems with tailored physical and chemical properties, which have been extensively summarized in the literature.[1–6] These presynthesized NPs can self-assemble into self-supported and organized structures or patterns, a process that occurs as a consequence of specific and local interactions between the components themselves and with no need of external guidance, although it can be assisted by external fields to achieve special arrangements, e.g., by applying magnetic fields,

light, ultrasound, *etc.* Self-assembly can be classified in plenty of ways, for example, distinguishing between so-called static and nonequilibrium or dynamic assembly.[7–9] In the first case, even if the formation of the ordered assemblies requires energy, once it is formed, it remains stable (the system evolves toward the global or local minimum of free energy). In the latter, the structures are formed away from equilibrium and require continuous energy input, disappearing when the external drive is removed. An example of the latter is the gelation process, where the small units suffer transformations until they reach nonordered, metastable structures.[10] The different strategies for the self-assembly of inorganic nanocrystals can be classified as follows: a) self-assembly in solution, b) using templating methods, c) solvent evaporation, and d) assisted assembly.[11] Nevertheless, the term self-assembly is really broad, which could involve noncovalent interactions of organic molecules in solution, growth of semiconductor quantum dots (QDs) on solid substrates, block copolymer superlattices, and so on.[12–15]

In this review, we summarize the recent efforts toward the assembly and superstructure formation of inorganic NPs used as building blocks, which would take place in an ordered or nonordered way. The review is therefore divided into "ordered assemblies," such as mesocrystals or superlattices, and "nonordered assemblies," focusing on NP-based gels. Each section contains a separate introduction appropriate to the topic, describing the driving force by which the respective assemblies take place and how the building blocks are arranged in the macrostructures. The arrangement of building blocks in ordered structures is made spontaneously by self-organization of the NP building blocks and with no need of external influences, whereas the arrangement of NP building blocks in nonordered structures is made arbitrarily, being necessary by the influence of an external trigger. Since a huge variety of different NP assemblies is accessible nowadays, both sections are subdivided according to the material or composition of their NP building blocks, e.g., semiconductor, magnetic, metallic, and hybrid, highlighting the latest findings in each field with reference to possible applications.

F. Lübkemann-Warwas, I. Morales, N. C. Bigall
Institute of Physical Chemistry and Electrochemistry
Leibniz University Hannover
Callinstraße 3a, 30167 Hannover, Germany
E-mail: nadja.bigall@pci.uni-hannover.de

F. Lübkemann-Warwas, I. Morales, N. C. Bigall
Cluster of Excellence, PhoenixD, (Photonics, Optics, and Engineering – Innovation Across Disciplines)
Leibniz University Hannover
30167 Hannover, Germany

2. Ordered Assemblies

The self-assembly of nanocrystals into ordered structures is a thermodynamically favorable process in which structural units, usually called building blocks, organize themselves into

**ADVANCED
SCIENCE NEWS**

www.advancedsciencenews.com

**small
structures**

www.small-structures.com

mesoscopic superstructures with well-defined symmetry and geometry.[16–20] The so-called building blocks can have different physical properties, sizes and may have complex shapes, so the possibilities and applicability of these systems are countless, even if not fully conceived yet. The main driving force of the formation of these ordered structures is the interaction energy between the structural subunits, which can be atoms, molecules, or particles. The focus of the research in the self-assembly falls on 1) the understanding of the physical mechanisms and the interactions involved in the different scales, 2) the synthesis of new structures, 3) fine-tuning the assembly's properties, and 4) the practical design for making smart materials and devices. By self-assembly, it is possible to organize the matter on larger scales while offering a huge control over the optical, mechanical, and electrical properties of the resulting material.[7] On top of that, it is not restricted to 2D structures, as it is the case of most of the physical top-down fabrication techniques of ordered assemblies, such as photolithographic and ion-implantation techniques, and the processing conditions are not as harsh, are less expensive, with no need of clean room facilities, not restricted capacity to achieve 3D structures and they overcome the poor resolution below 20 nm for the top-down techniques.[21]

In this section, we focus on different representative examples of ordered assemblies that can be created attending to the composition of the inorganic building blocks, such as semiconductor, magnetic, or metal nanocrystals, highlighting the different configurations they can adopt and the properties that arise. We will show how these building blocks can assemble into ordered structures and geometries, either nano-, micro-, or macroscopically. We will focus on colloidal ordered assemblies and colloidal superparticles (short-ranged ordered),[22] such as flowers, ribbons, needles, chains, and highly uniform in size spherical assemblies, also showcasing examples of long-range ordered assemblies such as superlattices and mesocrystals. It is shown that rational design leads to countless synthesis possibilities and applications, attending to the composition of the building blocks, its physical and chemical properties, their size and shape, the surface ligands, the solvents, and the proper reaction conditions.

2.1. Semiconductor Building Blocks

Dubertret et al. successfully synthesized semiconductor nanoplatelets (NPLs) with well-controlled shapes and sizes at the atomic level.[23] Since then, many works have reported that nanocrystals in the form of platelets, regardless of their composition, have the tendency to form columnar assemblies, based most frequently on van der Waals attraction forces, but also on dispersive, osmotic forces or long-range magnetic dipole interactions.[24–29] In particular, due to their anisotropic shape, semiconductor NPLs are quite prominent examples of ordered assemblies, as will be seen in this section.

In 2013, for the first time, the self-assembly of semiconductor CdSe (NPLs) into ordered stacks (in the thickness direction) was reported. Due to the NPLs' anisotropic 2D geometry, 1D superlattices could be formed.[30] The control over the stacking was achieved by the correct choice of the solvent and the measurement protocol, while it has also been reported that the amount and nature of the surface ligands play a fundamental role in the

way the NPLs stack.[27,31,32] Basically, when the NPLs were dispersed in pure hexane, no stacking occurred, and the NPLs were well dispersed. However, when a small amount of a polar anti-solvent (ethanol) was added to the solution, the increase in the polarity favored the arrangement of the NPLs one on top of each other to diminish their surface contact of the NPL ligands with the solvent. The optical properties of the stacked NPLs were found to be different from that of the single NPLs and of the nonordered assemblies of NPLs, as can be seen by the appearance of an additional red-shifted emission peak in the photoluminescence (PL) spectra at 20 K, attributed to the longitudinal optical phonon emission line. After that pioneer work, other groups have investigated the stacking of semiconductor NPLs and their properties[33,34] with potential application in optoelectronic devices due to the NPLs' emission of polarized light,[35] in light-harvesting[36] or in photoelectrochemical sensing.[37]

One recent work in the self-assembly of ordered CdSe and CdSe/CdS-based core/crown NPLs[38] focused on distance minimization to enhance electronic transport within the stacks. In this work, polymer encapsulation of NPL stacks is carried out, which improves the colloidal stabilization of the stacks, facilitates the water transfer, and allows to reduce further the NPL distance.[39] The study was carried out for different NPL heterostructures: CdSe/CdS-core/crown type-I, CdSe/CdTe core/crown type-II, and CdSe/CdS core/shell quasi-type-II. The distances were tuned by means of ligand exchange (**Figure 1**a 1–4), replacing the native carboxylic acid long chains with shorter amine ligands and $CdBr_2$. They report that by increasing the amount of $CdBr_2$, the NPL distance is shortened (Figure 1a 5–9). The unprecedented reduced distance between NPLs achieved in this work (less than 1 nm) translates into much higher photocurrent densities and especially photocurrent transport through the stacks. In recent years, there are plenty of research efforts devoted to increase the charge transport effectivity in these assemblies to enable and boost their practical use in optoelectronic devices, for example, by their collective assembly in films[40] with the NPLs oriented either edge-up (with the NPLs in each layer fully stacked) or face-down (nonstacked).[41–45] These orientational control of the NPL-shaped NCs can be achieved by the widely used liquid-air self-assembly technique. By repeating the NPLs deposition process sequentially, highly uniform and superstructured multilayers can be obtained. These structures out of CdSe/CdZnS core–shell NPLs allow the development of large-area optically active planar waveguides (Figure 1b).[41] In that work, the authors additionally showed that the optical gain achieved in these NPL film assemblies allows to reduce the organic barriers, beneficial for their application in electroluminescence devices because the presence of organic ligands acts as insulators hindering the charge or heat transfer. From a fundamental point of view and with the aim of improving the efficiency of semiconducting NPL lasers, photodetectors, and nanocrystal solar cells, other works focus on the understanding of the dipole–dipole interactions between the NPL in monolayers (Figure 1c).[42,44] It is shown that the dipole interaction of the NPLs in an additional tool to control the Förster resonance energy transfer, which depends on the dipole orientation and inter-NPL distances, observing different PL decay dynamics if the NPLs are structured face-down (slower PL decay) or edge-up in the monolayer.
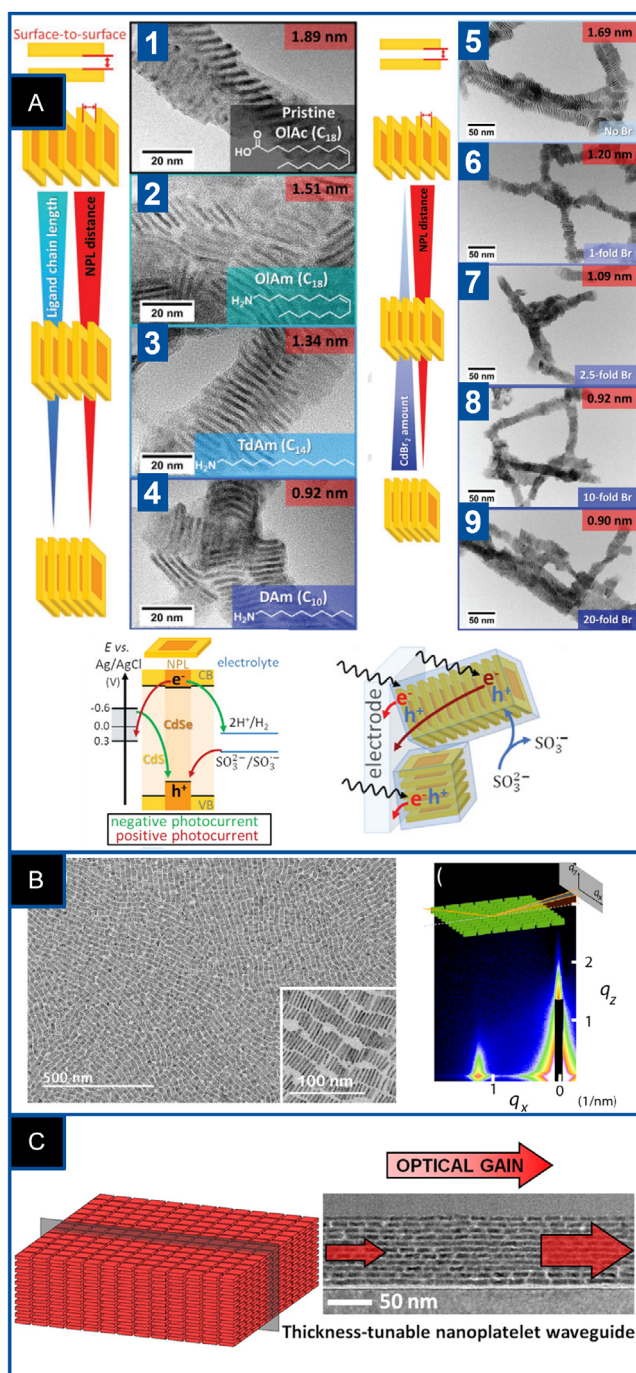
**ADVANCED
SCIENCE NEWS**

www.advancedsciencenews.com

**small
structures**

www.small-structures.com

Figure 1. Self-assembly of semiconducting building blocks into ordered stacks and films. a) TEM images of polymer encapsulated CdSe/CdS core-crown NPL stacks. NPL–NPL distance changes by changing the length of the ligands (left) and by the addition of $CdBr_2$ to a constant amount of decyl amine (DAm) (right). Bottom: possible charge carrier transport and transfer processes in the NPL stacks. Adapted with permission.[38] Copyright 2022, Wiley–VCH GmbH. b) Scheme and cross-sectional TEM image of highly uniform 11 NPL layers in silicon. Adapted with permission.[41] Copyright 2020, American Chemical Society. c) TEM images of CdSe NPLs monolayer films with edge-up configuration and GIXAS (grazing incident small-angle X-ray scattering) pattern for the edge-up assembly showcasing a strong lateral scattering peak. Adapted with permission.[42] Copyright 2017, American Chemical Society.

Moreover, not only ordered stacks of flat NPLs have been reported so far.[46] Jana et al.[31] showed the assembly of semiconductor CdSe NPLs into twisted ribbon superstructures upon the addition of oleic acid and drying in different steps (**Figure 2**a). They also observed the surface distortion of individual NPLs due to the surface strain caused by the increase in the ligand coverage, going from flat to a twisted shape (Figure 2a), which leads to ribbons where the individual twist propagates over the whole length. A later article deepened into the understanding of these chiral structures and mechanisms while putting forward strategies for the improvement of their optical properties for their use in optoelectronic devices.[47] In the line of chiral structures, a recent article proposed a method to assemble semiconductor CdTe NPs into helices for chiroptical activity in the NIR (Figure 2b), evaluating the influence of the solvent, the pH or the ligand density into their assembly, with potential application in microelectromechanical systems, optofluidic devices or mechanical metamaterials, among others.[48] In this work, the authors observed that the coordination bonds between the Cd^{2+} and the cysteine used as surface ligands might be one of the reasons for exerting chiral bias on the NP–NP interaction. More works on self-assembly into ordered chiral structures and their potential applications can be found in this comprehensive review,[49] showcasing the importance and necessity of ordered assemblies of inorganic NPs to enable promising applications. Another example of the potential of the self-assembly of semiconducting building blocks can be found in Figure 2C. In that work,[35] the authors reported the assembly of CdSe NPLs into long anisotropic microneedles by the addition of an antisolvent to the NPL colloidal solution (Figure 2c-left). The NPLs were oriented perpendicular to the long axis of the needle, displaying polarized light emission (Figure 2c-right). Another microneedle-like superparticle was obtained from CdSe/CdS semiconductor nanorods (NRs) by incubating them with octylamine for 6 days under Ar, indefinitely stable in strong polar solvents and interesting for building polarized light-emitting diodes.[50]

Different final geometries can also be achieved by the proper selection of the initial shape and size of the building blocks and the synthesis conditions, arising unique optical, electrical, and mechanical properties. For example, the self-assembly of colloidal semiconductor nanocrystals into superlattices has also been achieved and can be found elsewhere.[51,52] In the case of the hierarchical self-assembly of CdSe monodisperse colloidal octapods,[52] it has been observed that the branched NCs self-assemble first into linear chains and later into 3D porous superstructures (Figure 2d). For tetrahedral CdS nanocrystals, it has been reported their spontaneous organization into self-assembled superlattices, less dense than expected for the packing of perfect tetrahedra.[53] This is due to the predominant vertex-to-vertex contact (instead of face-to-face) between the nanotetrahedral crystals, driven by the ligand–ligand interaction forces.

2.2. Magnetic Building Blocks

For the self-assembly of magnetic nanocrystals, nature has a very inspiring example: the magnetotactic bacteria (**Figure 3**a). This microorganism naturally synthesizes magnetite NPs, called magnetosomes, with very low dispersity of sizes, shapes, and
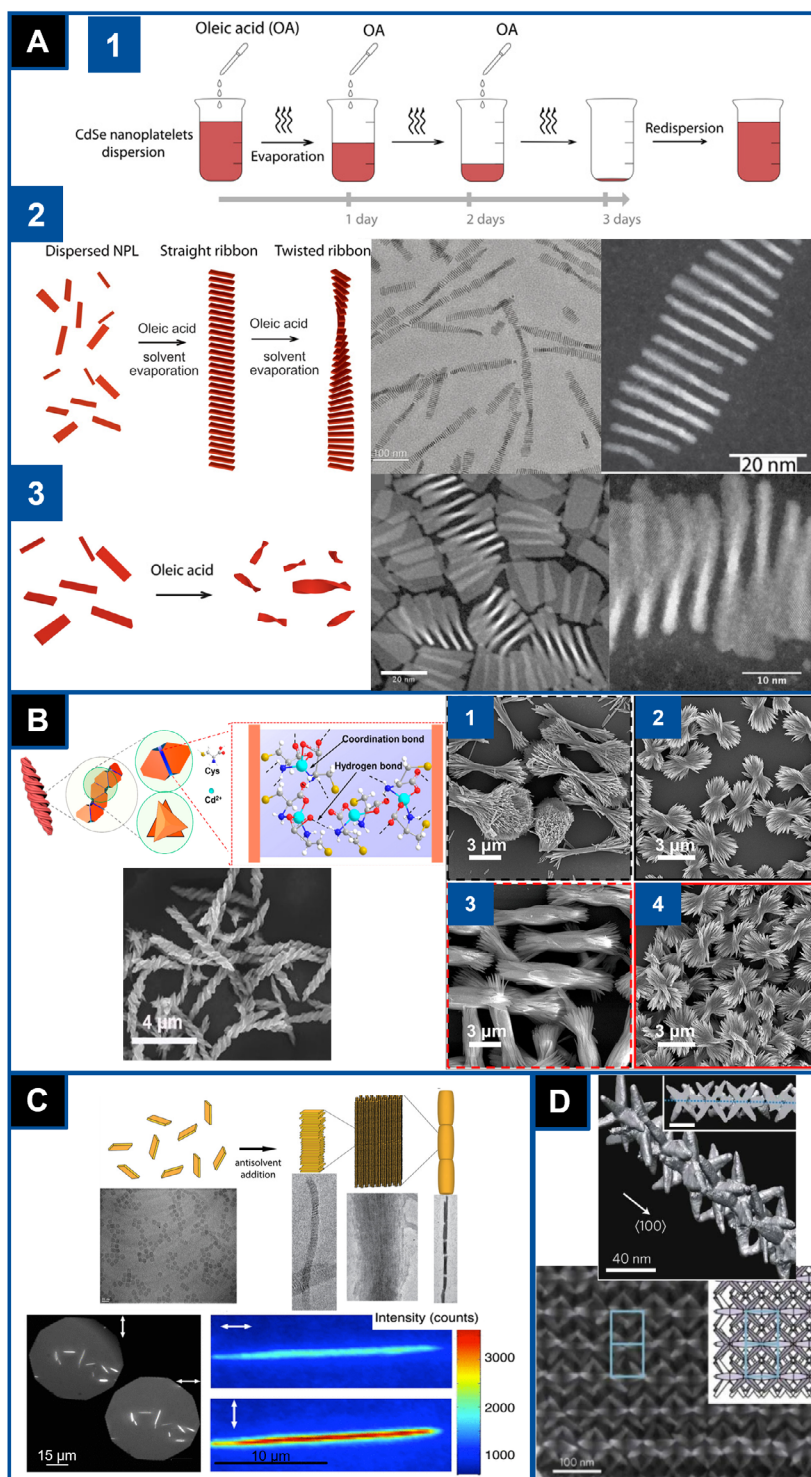
Figure 2. Examples of self-assembly of semiconducting building blocks into twisted stacks, superlattices, and microneedles. a) Scheme of the procedure to obtain twisted ribbons (1), scheme and HAADF-STEM images of twisted CdSe ribbons (2), and twisted NPLs (3). Adapted with permission.[31] Copyright 2017, The Authors, some rights reserved; exclusive licensee AAAS. Distributed under a CC BY-NC 4.0 license http://creativecommons.org/licenses/by-nc/4.0/?. Reprinted with permission from AAAS. b) CdTe chiral nanoparticles self-assembly into highly monodisperse helices. Bow-tie assemblies in different media incubated at 37 °C for 3 days: 1 and 3 in aqueous solution with L-cys and D-cys, respectively, 2–4 in a mixture of water and methanol with L-cys and D-cys, respectively. Adapted with permission.[48] Copyright 2019, American Chemical Society. c) Microneedle formation by the stacking of CdSe NPLs (left) and visualization of the light emitted by the needles depending on their orientation with respect to the polarizer (right). The light emitted is strongly polarized in the direction perpendicular to their long axis. Adapted with permission.[35] Copyright 2013, American Chemical Society. d) CdSe octapods self-assembly into chains and superlattice structure formed by the assembly of the preformed chains. Adapted with permission.[52] Copyright 2011, Nature Publishing Group.

very high (structural, chemical, and magnetic) quality, arranging them into chains, a mechanism mediated by proteins and magnetic dipolar interactions.[54] This arrangement of magnetic NPs into chains has an enormous interest in the field of magnetic hyperthermia, as it has been reported to increase significantly the heating efficiency (Figure 3a).[55–57] In addition, taking advantage of the magnetic properties of the building blocks, the self-assembly can be assisted by an external magnetic field. While in equilibrium self-assembly, there is a global minimum in the free energy landscape; when a magnetic field is applied, the magnetic NPs are kinetically trapped and assembled in a local minimum (Figure 3b). In the case of FeCo/Co_2Fe_4 core–shell NPs, under an applied magnetic field, the minimization of the local magnetostatic energy translates into their arrangement into chains in the superlattice[58] (Figure 3b).

There are several works reporting the self-assembly of magnetic nanocrystals into chains (Figure 3c),[59,60] also by triggering
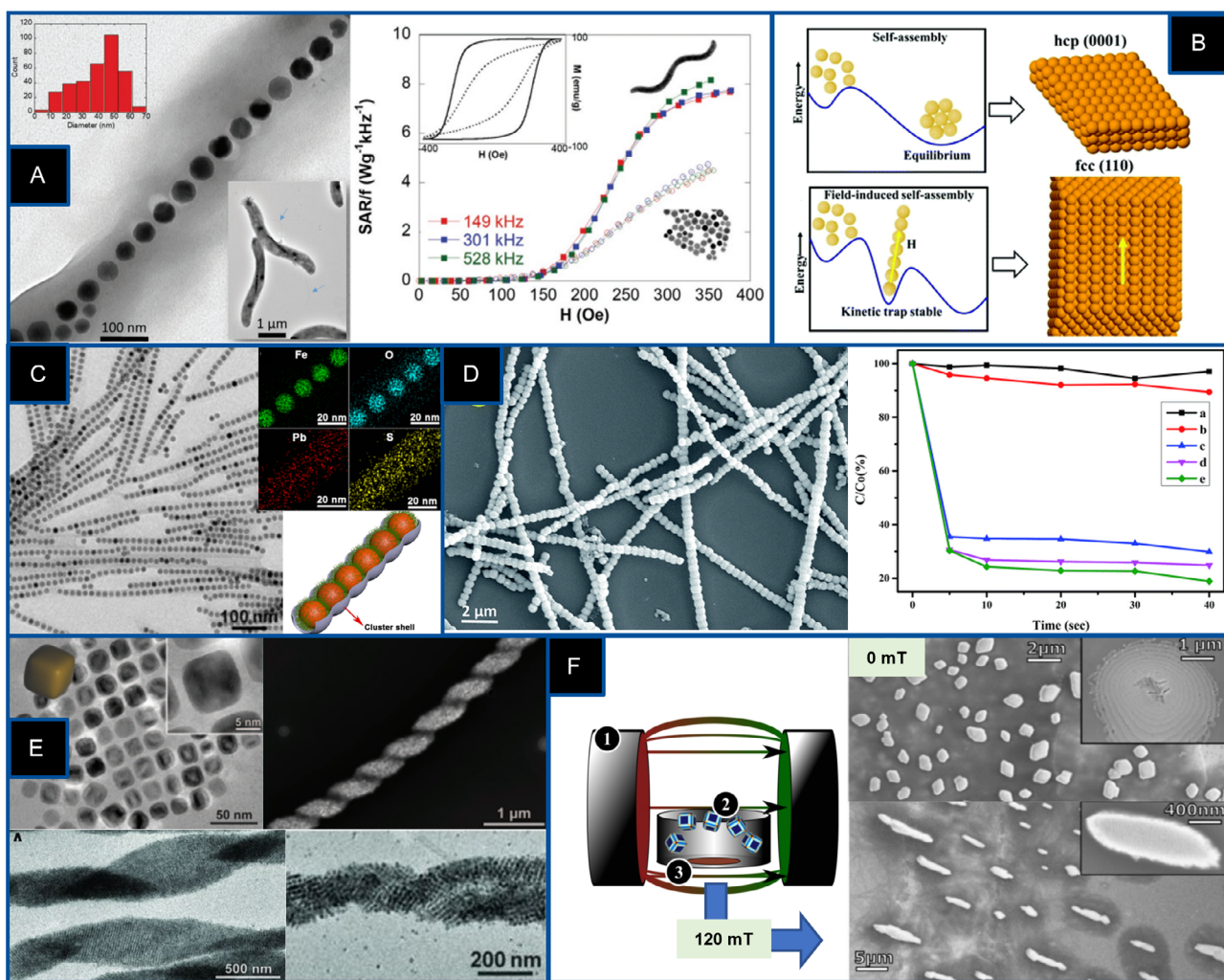

Figure 3. Examples of self-assembly into chains or elongated ordered structures of magnetic building blocks. a) TEM image of the chain of magnetosomes inside *M. gryphiswaldense* MSR-1 bacteria. Inset: whole bacteria (left). Comparison of the heating efficiency of the magnetosomes in chains vs. the magnetosomes dispersed in water (right). Adapted with permission.[56] Copyright 2019, The Authors. Published by WILEY-VCH Verlag GmbH & Co. b) Free energy landscape of the self-assembly process of FeCo/$CoFe_2O_4$ nanoparticles in the absence or in the presence of an external magnetic field (left) and the superlattice structures thereof. Adapted with permission.[58] Copyright 2021, The Royal Society of Chemistry. c) TEM image of chains of magnetite (Fe_3O_4) NCs reassembled by switching the solvent from chloroform to hexane. Elemental mapping of one chain showing the encapsulation of the NC chains by a half-cylindrical cluster (right). Adapted with permission.[217] Copyright 2016, American Chemical Society. d) Fe_3O_4@P(MAA-DVB) magnetic nanochains self-assembled by polymerization under an external magnetic field (left). Fe_3O_4@P(MAA-DVB)-Pd(0) degradation of Rhodamine B (right). Black and red lines stand for the absence of catalyst and the nanochains without Pd. Adapted with permission.[218] Copyright 2016, The Royal Society of Chemistry e) Top: TEM image of rounded Fe_3O_4 cubes and SEM image of the helical superstructure self-assembled from the cubes. Bottom: TEM image of an individual single-stranded helix (left) and of a double helix (right). Adapted with permission.[61] Copyright 2014, reprinted with permission from AAAS. f) Self-assembly of Fe_3O_4 nanoparticles into mesocrystals by evaporation of the solvent under a homogeneous magnetic field. Scheme of the set-up (1—electromagnet, 2—nanoparticle solution, 3—TEM grid) and final mesocrystals with no applied field (top) and with 120 mT of the applied field (down). Adapted with permission.[65] Copyright 2019, Beilstein-Institut.

the chain formation by means of an externally applied field (Figure 3d–f).[61–64] In a very interesting article, the authors self-assembled superparamagnetic magnetite nanocubes into helical superstructures in a template-free way (Figure 3e) by solvent evaporation in the presence of a magnet and studied the interactions and forces that lead to this chiral chain clusters.[61] Other interesting work on the magnetic field-assisted assembly of superparamagnetic NPs can be found here,[65] where the authors reported the fabrication of anisotropic mesocrystals elongated in the direction of the applied field (Figure 3f).

Regarding the interest in having colloidal ordered magnetic assemblies (COAs) for biomedical applications, Bigall et al. synthesized manganese iron oxide nanobeads, arrangements of well-ordered superparamagnetic nanocrystals (**Figure 4**a), with and without amphiphilic polymer coating, and studied how the arrangement of the NPs changed as a function of the polarity of the destabilizing agent.[66] In this work, the authors improve the synthesis method with respect to their previous work,[67] separating the aggregation step of the NPs into close-packed ordered assemblies and the polymer encapsulation step. They observed that the systems were still in the superparamagnetic regime after the assembly and showed that the polymer-nanobeads assemblies had a higher mobility under the action of external magnetic fields, which makes them interesting materials for applications such as magnetofection or magnetically driven drug delivery. They proved that these polymer-coated colloidal ordered assemblies have a potential application as T_2 contrast agents for magnetic resonance imaging (MRI) due to their high r_2 relaxivities. Another system that has been reported to be a good T_2 contrast agent for MRI combined with anticancer activity is the self-assembled porous Mn-doped Fe_3O_4 NPs, in which the particle size and porous structure were controlled by the amount of water added.[68] Interestingly, the self-assembly of NPLs building blocks does not always lead to columnar ordered or twisted stacks. It has been shown that Ni hexagonal NPLs (Figure 4b)[69] and Co NPLs[70] can assemble into spherical flower-like 3D structures with potential applications as magnetic data storage devices and catalysts. Another ordered assembly suitable for electrocatalysis can be found here.[71] Briefly, by a combination of template-mediated epitaxial growth, confined assembly, and oriented attachment mechanism, it is possible to obtain frame-like superstructures, as shown in Figure 4c. Fe-Co Prussian blue analog NPs are used as building blocks, which are known for having switchable magnetic and electronic properties, obtaining ordered 3D architectures with highly open structures. After thermal treatments, Co–Fe-mixed oxides are obtained, proving to be efficient as electrocatalysts for oxygen reduction reactions (ORR). Finally, more works on the self-assembly of magnetic nanocrystal building blocks can be found in this interesting review,[72] where the authors also address their potential use as nanoscale electronic devices, sensors, high-density data storage media, and biomedical theragnostic systems.

2.3. Metallic Building Blocks

The self-assembly of noble metal nanocrystals has attracted a lot of attention due to their strong interaction with electromagnetic fields and their collective and emerging optical properties.[73]

Sánchez–Iglesias et al. synthesized ordered clusters of amphiphilic polymer-coated Au spherical nanocrystals by solvent-mediated reversible self-assembly (**Figure 5**a), tuning the cluster size and the particle–particle distance with the proper choice of Au NCs diameter and the length of the hydrophobic polymer chains (polystyrene).[74,75] By adding water to the tetrahydrofuran (THF) solution containing the Au NCs, the optical response of the assembly changed, reflected in the change of the color of the colloid and in the shift of the maximum of the localized surface plasmon resonance (LSPR). They found that the increase of the length of the polystyrene chain increases the redshift of the plasmon band regardless of the mean diameter of the Au NPs, due to the larger size of the Au cluster with decreasing volume fraction (which translates into a higher number of contributing particles). In brief, the redshift originates from the collective interactions of the particles with light. As mentioned before, the authors used an amphiphilic diblock copolymer to stabilize the clusters and prevent their uncontrolled precipitation as a model for the use of other biodegradable copolymers for application as drug delivery carriers. In later works, the authors further study these clusters and how to tune their properties and prepare binary clusters composed of Au nanocrystals of two different sizes[76] and different shapes.[77]

A very interesting example of the self-assembly of plasmonic NCs in which also a change in the plasmonic resonance is observed can be found here.[78] The authors self-assemble Au@Ag NCs into nanosheets (which showcase analogous properties to graphene) and fold them into desired origami 3D structures by means of focus ion beam lithography (Figure 5b), observing a blue shift of the plasmonic peak and a narrowed bandwidth in comparison to the unfolded sheet. These structures have potential applications as foldable and flexible plasmonic devices, plasmonic waveguiding, and sensing.

Moreover, Au NPLs can self-assemble into spheres, cauliflower- or mushroom-like superparticles[79] (Figure 5c). For that, the authors used an aniline derivative (NAAN) to reduce the gold precursor ($HAuCl_4$) in the presence of bromide, and depending on the reaction conditions, the different structures were obtained. In particular, the ratio between the $NAAN/HAuCl_4$ plays a crucial role: when the ratio is low (8/1 or below), the formation of mushroom-like Au superparticles takes place. They demonstrate that the driving force for the self-assembly is the $\pi–\pi$ stacking interaction and show that these Au superstructures are excellent materials for surface-enhanced Raman scattering (SERS) substrates for detecting organic molecules, as they generate intense SERS signals under different laser excitation conditions. For this application, recent articles also report that the self-assembly of Au octahedra array is very reliable SERS substrate and thus useful for cancer diagnosis and treatment,[80,81] similar to 3D self-assembled structures of photonic crystal beads from silica-coated Ag NPs.[82] An interesting biomedical application for lung cancer diagnosis was reported here,[80] using Au superparticles surrounded by ZIF-8 MOF (Figure 5d). The authors developed a detector with high sensitivity and high selectivity toward aldehydes, a lung cancer biomarker promising for early-stage lung cancer detection.

As has been seen, metallic nanocrystal-ordered assemblies are particularly interesting for improving surface-enhanced spectroscopy due to their LSPR, which allows their use in fields such as
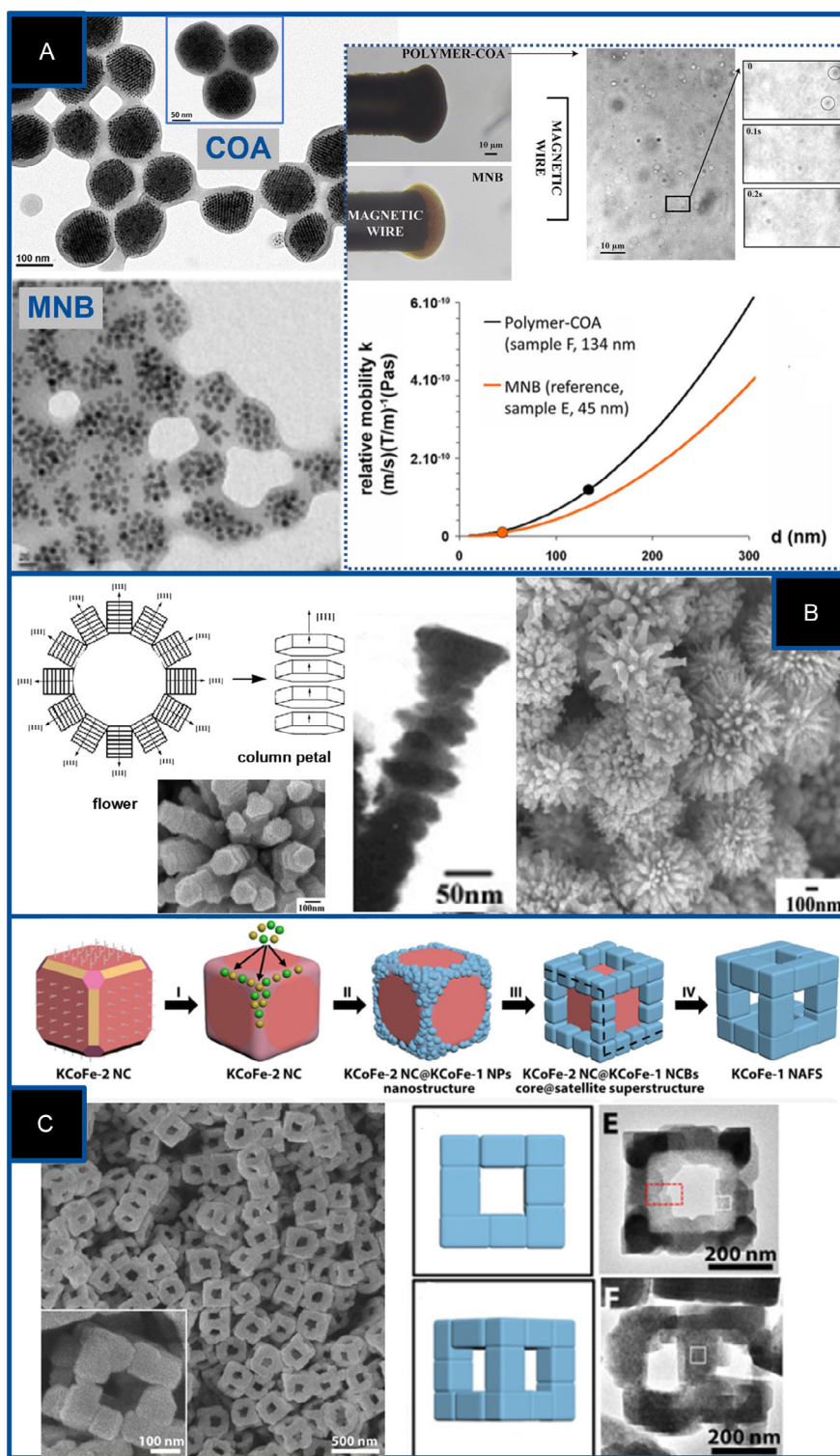
ADVANCED
SCIENCE NEWS

www.advancedsciencenews.com

small
structures

www.small-structures.com

Figure 4. Examples of self-assembly of magnetic building blocks. a) TEM images of polymer-coated colloidal ordered assemblies (COAs) and nonordered magnetic nanobeads (MNB) of manganese iron oxide (left). Magnetophoretic measurements of polymer-COA vs. MNB and magnetic relative mobility *k* as a function of the diameter for the polymer-COA and MNB (right). Adapted with permission.[66] Copyright 2013, American Chemical Society. b) SEM image of self-assembly of hexagonal-shaped Ni platelets into a 3D flowerlike assembly. Amplified image of the columnar nanoplatelets emerging from the center. Adapted with permission.[69] Copyright 2007, American Chemical Society. c) Schematic illustration of the formation mechanism of a nanocuboid-assembled frame-like superstructure (NAFS) (top), FESEM image of the KCoFe NAFS (left), and schematic model at two orientations and TEM images of the structures (right). Adapted with permission.[71] Copyright 2017, The Authors, some rights reserved; exclusive licensee AAAS. Distributed under a CC BY-NC 4.0 license http://creativecommons.org/licenses/by-nc/4.0/. Reprinted with permission from AAAS.

**ADVANCED
SCIENCE NEWS**

www.advancedsciencenews.com
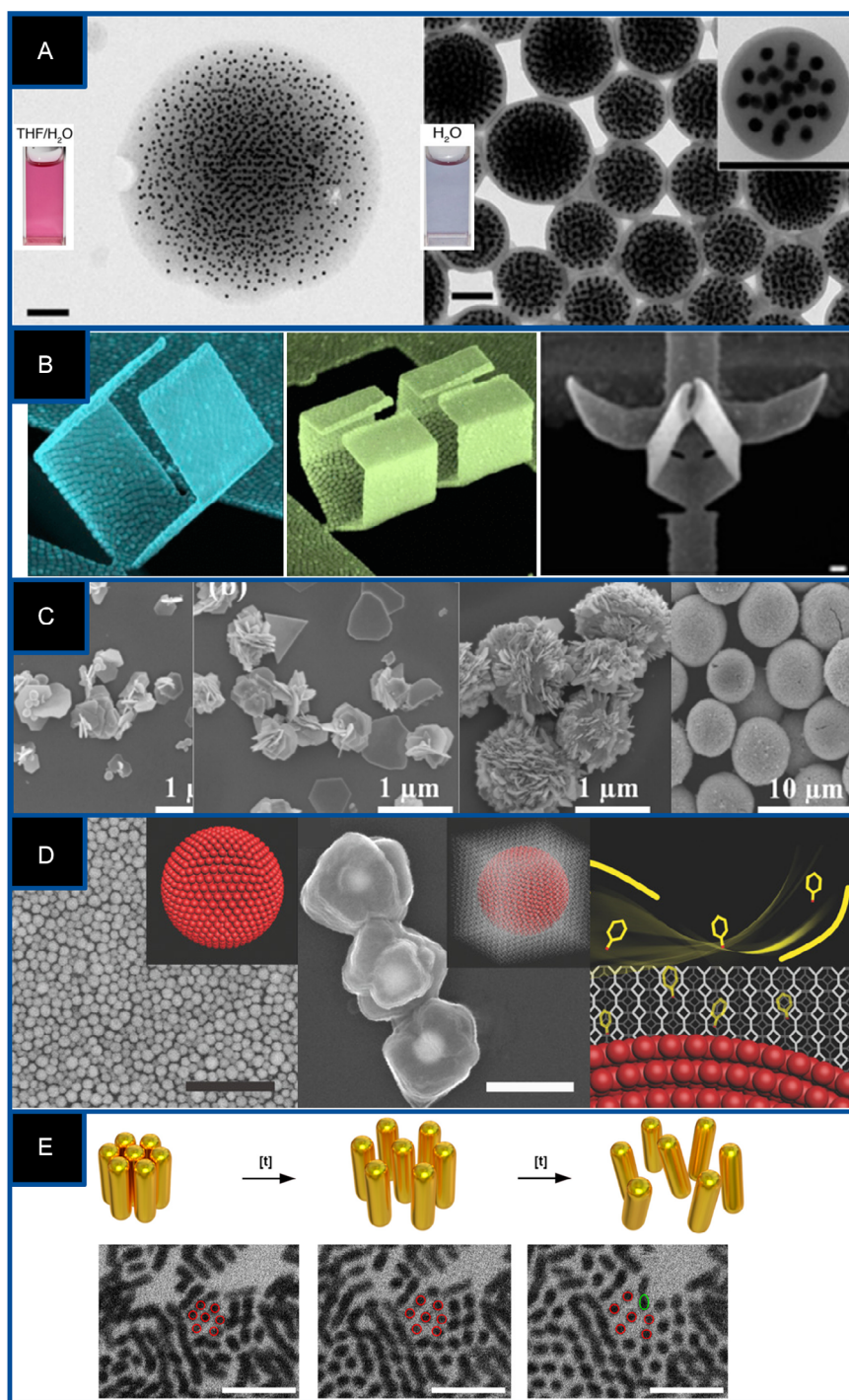
**small
structures**

www.small-structures.com

Figure 5. Examples of self-assembly of metallic building blocks. a) TEM images of Au@PS-b-PAA clusters: stable and bigger assembly in a mixture of THF and water (top-left) and after a mild thermal treatment at 70 °C and water transfer, which leads to more rigid and ordered cluster with reduced size (top-right). Scale bar 200 nm. The insets show the change in the color of the colloids depending on the solvent. Adapted with permission.[75] Copyright 2012, American Chemical Society. b) SEM images of plasmonic origami 3D structures self-assembled from Au@Ag NCs. First, the nanosheets are formed and are later folded by means of focused ion beam (FIB) lithography. Scale bar 200 nm. Adapted with permission.[78] Copyright 2014, American Chemical Society. c) SEM images of the assembly of the NPLs into spheres were obtained at 2, 5, 10, and 30 min from left to right (bottom). Adapted with permission.[79] Copyright 2020, Elsevier Inc. d) Left: SEM image of the gold superparticles (scale bar 1 μm), center: SEM of the gold superparticle with ZIF-8 around and right: schematic representation of the detector gas collisions and gas absorption process for the gold superparticles with the ZIF-8. Adapted with permission.[80] Copyright 2017, John Wiley & Sons, Inc. e) Scheme of the assembly and disassembly of gold nanorods functionalized with MUDOL and STEM images at different times showing the assembly and disassembly (video in the original article). Adapted with permission.[84] Copyright 2020, American Chemical Society.

**ADVANCED
SCIENCE NEWS**

www.advancedsciencenews.com

**small
structures**

www.small-structures.com

photonics and sensing. Nevertheless, there are still different challenges ahead. One of them is the preparation method of efficient nanocrystals, which normally are hydrophilic and unsuitable for SERS. In that regard, further research in the correct functionalization of the NPs as well as in the preparation of the SERS substrates is necessary.[83] Also, the stability of the substrates must be improved to avoid the signal decrease, as well as their reusability. The biomedical application of these structures based on SERS is still very scarce, and a good coupling between the analytes and to the plasmonic surface is needed. Another of the challenges is to obtain uniform, highly reproducible, and more efficient structures, in which the efforts toward new and more precise assembly techniques and a further understanding of the self-assembly process in the nanoscale will be pivotal for the commercialization of such nanoplatforms.

To overcome one of the main challenges and shed more light into the assembly process of the metallic NCs themselves, as well as to control it, different works have put effort into the in situ observation of the assembly formation.[84–86] By means of in situ environmental STEM, combined with UV/Vis spectroscopy, small-angle X-ray diffraction, and multiscale modeling, Grzelak et al. reported a detailed picture of the stimuli-responsive self-assembly dynamics of gold NRs (Figure 5e).[84] Finally, due to the undoubted versatility of the self-assembly to obtain ordered structures, several assemblies out of different shaped metallic building blocks can be obtained, for example, from cubes,[87] octahedrons,[88] or tetrahedrons.[89,90]

2.4. Hybrid Building Blocks

Using nanocrystals with different sizes, shapes, and compositions, it is possible to create highly ordered hybrid superlattices.[91–94] This allows to design of new functional metamaterials with the possibility of tailoring their properties by the proper control of the nanocrystal interactions within the assembly. Binary superlattice structures, with high orientational and positional order, composed of rhombic GdF_3 and tripodal Gd_2O_3, have been synthesized by shape-directed self-assembly (**Figure 6**a).[95] The shape complementary of the building blocks gives place to stable interlocked structures via shape-specific directional interactions. Other examples of binary superlattice can be found here,[96] where the authors reported the self-assembly of $\Upsilon\text{-}Fe_2O_3$ nanocrystals and PbSe semiconductor QDs. Recently, Kovalenko et al. reported the fabrication of perovskite binary and ternary nanocrystal superlattices via shape-directed coassembly using cubic $CsPbBr_3$, spherical Fe_3O_4, or $NaGdF_4$ nanocrystals and truncated-cuboid PbS.[97] They reported that the superlattices showcase a high degree of orientational ordering and that they exhibit superfluorescence, which could make these structures interesting as ultrabright quantum light sources. Shortly later, they published a comprehensive study of all the different structures that can arise from the multicomponent NC superlattices made out of lead halide perovskite nanocubes.[98]

Regarding colloidal ordered assemblies, the synthesis of self-assembled trimetal Ag@AuCu nanoplates (Figure 6b) has been reported.[99] The authors synthesized multibranched AuCu nanostar alloys, using $CuCl_2$ and $HAuCl_4$ as precursors, hexadecylamine to stabilize the nanocrystals and glucose as reducing

agent, and the nanostars branch number and length are determined by the atomic ratio of Cu in the precursors. Afterward, adding different amounts of $AgNO_3$ leads the hybrid nanostructures clustered together and self-assembled, acquiring trigonal or hexagonal morphologies (between 3 and 5 μm average side length), which depended on the amount of silver nitrate added. Also, by increasing the reaction time, they observe the change from a porous bigger structure to a denser and shrunk structure. Another example of hybrid self-assembled colloidal ordered nanostructure can be found here,[100] where the authors obtained colloidal magnetoplasmonic assemblies of Au nanostars and iron oxide NPs encapsulated in an amphiphilic polymer (Figure 6c), a system highly responsive to light and external magnetic fields, demonstrating that hydrophobic interactions are the driving force toward the self-assembly.

Beyond superlattices and colloidal ordered assemblies, mesocrystals are also an interesting class of highly packed assembled structures with long-rage order at the atomic level in at least one dimension, with applications in photo/electrocatalysis, energy conversion, and storage.[101] Recently, the Cölfen group reported the first description of the preparation and characterization of highly ordered 3D binary mesocrystals by simultaneous self-assembly of platinum and iron oxide nanocubes. They demonstrate that by a gas-phase diffusion technique, it is possible to randomly incorporate platinum nanocubes into an iron oxide host lattice (Figure 6d).[102]

There are several works reporting the fabrication of hybrid nanostructures also by templated self-assembly, using patterned objects, which will serve as scaffolds where the NPs can arrange into controlled morphologies.[103,104] The templates can be made by lithographic techniques,[105] atomic layer deposition, electrodeposition, DNA or virus scaffolds, etc. Other way to obtain hybrid nanostructures is the droplet evaporative self-assembly technique used in this work[106] to synthesize superlattice arrays of Au NRs and Fe_3O_4 NPs on a porous Teflon membrane. For that, a drop of a mixture containing highly concentrated AuNRs with Fe_3O_4 NPs is dripped into a treated Teflon platform. The Teflon is treated with a perfluorinated fluid (to make the surface slippery). The subsequent evaporation and condensation of the droplet lead to the self-assembly of the hybrid NPs, which have proved to be a very interesting magnetoplasmonic surface for SERS detection of environmental pollutants, with the advantage of being possible to manipulate it with an external magnetic field, allowing a rapid separation of the analytes and yielding high sensitivity.

Summarizing, the self-assembly of nanocrystals into 1D,[107] 2D, or 3D structures[108] (either microscopic or macroscopic and self-supported or templated) is a research field that has attracted a lot of interest in the last years, with a lot of projection and with plenty of room for improvement and new designs of novel multifunctional materials.

2.5. Summary and Outlook Ordered Assemblies

In the field of ordered assemblies, one of the main challenges is to understand which external factors are affecting the superstructure formation as well as preserving the periodicity and long-range crystalline order. For example, to obtain long-range
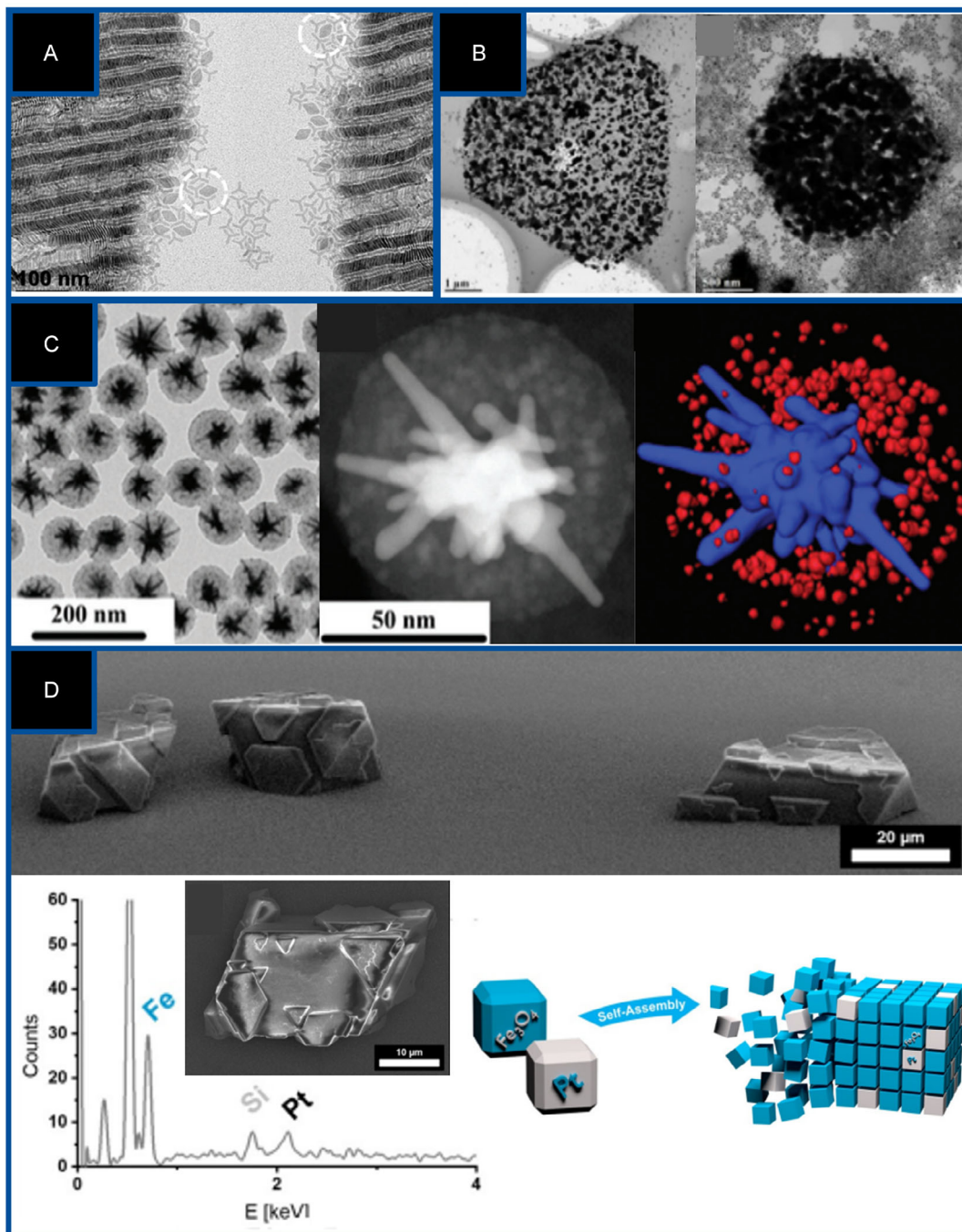
Figure 6. Examples of self-assembly of mixed building blocks. a) TEM image of shape-complementary self-assembly of Gd_2O_3 tripodal nanoplates and GdF_3 rhombic into a binary superlattice. Adapted with permission.[95] Copyright 2013, American Chemical Society. b) TEM images of AuCu nanocrystals coated with Ag, self-assembled into hexagonal plates: low dense (left) and high dense (right), depending on the reaction time. Adapted with permission.[99] Copyright 2020, MDPI. c) Hybrid colloidal assemblies of Au nanostars and Fe_3O_4 nanoparticles: TEM image of the magnetoplasmonic assemblies after encapsulation in an amphiphilic polymer (left), HAADF-STEM (middle) and 3D tomography reconstruction of an individual cluster (right). Adapted with permission.[100] Copyright 2015, Royal Society of Chemistry. d) SEM image of binary superstructures in hexane formed by Pt incorporated into an iron oxide mesocrystaline host lattice (top). EDX analysis of one binary crystal and scheme of the assembly (bottom). Adapted with permission.[102] Copyright 2021, The Authors. Angewandte Chemie International Edition published by Wiley-VCH GmbH.

crystalline order, different assembly techniques can be used, like the lithography-free approach,[109] to fabricate large-area assemblies that maintain long-range order in close-packed arrangements, by engineering it[110] or by oriented attachment,[111] among others.

On the other hand, to obtain ordered structures and for many of the applications discussed before, frequently it is necessary to transfer colloidal nanocrystals onto solid substrates. Therefore, one of the present challenges is the upscaling of films toward long-range and large-scale homogeneous assemblies ($>>\mu m^2$), as well as their integration into devices.[40]

Improving the nanocrystal synthesis and the correct functionalization for the desired application, along with a deeper understanding of the growth process itself, will be crucial for the further development and commercialization of platforms based on ordered nanocrystal assemblies. Due to its importance, recent works have put efforts into a deeper understanding of the assembly of inorganic nanocrystals in ordered assemblies by in situ tracking the assembly process.[84,112]

Finally, it is worth mentioning that along with semiconducting, metallic, and magnetic building blocks, nowadays, there is an increased research interest toward the self-assembly of perovskites into ordered structures[113–116] due to their interest in optoelectronic devices.

3. Nonordered Assemblies

Compared with ordered assemblies, the self-assembly of individual nanocrystals into macroscopic and mostly nonordered structures represents a unique class of materials. One of the most prominent classes of nonordered assemblies are gels which exhibit high specific surface areas, low densities, and rapid mass transport pathways.[117–122] A gel can be made out of any material, and usually, it consists of long-chain macromolecules or interconnected nanocrystal building blocks and a dispersed phase. Nowadays, the aerogel community uses many different terminologies for such gel networks depending on the applied drying technique or the nature of the dispersed phase. In general, a gel structure in which the dispersed phase is air is called aerogel. If the dispersed phase is any kind of solvent, they are called lyogels or solvogels; however, in the case of water, they are called hydrogels, and in the case of alcohol, they are named alcogels. In addition, pending the applied drying technology, gel structures can also have different notations. Classically, aerogels are obtained using a supercritical drying process developed by Kistler in 1931.[123] First, the initial solvent has to be replaced by a solvent whose critical point is in a technically accessible temperature and pressure range, e.g., liquid CO_2 (31.1 °C and 73.7 bar). Second, within an autoclave and by increasing temperature and pressure above the critical point of the solvent, the transition from a liquid phase to a supercritical fluid without crossing a phase boundary takes place. Finally, to achieve the transformation of the supercritical fluid to the gashouse phase without crossing a phase boundary, the pressure is decreased at a constant temperature. Xerogels are obtained by evaporation and drying of the solvent under ambient conditions resulting in a significant shrinkage of the network due to strong capillary forces occurring at the interface of the solvent and the network. Cryogels or Cryoaerogels are received using freeze-drying or lyophilization, where the solvent within the gel structure is first frozen, followed by removing the frozen solvent by sublimation. In general, to control the self-assembly of nanoparticle building blocks into macroscopic nonordered NP-based gel structures and to bridge the nanoscopic and the macroscopic world, nowadays, a

myriad of destabilization approaches for different kinds of NP building blocks are established.[118–122] The most common destabilization procedures are based on the removal of NC surface ligands by chemical[124–129] or photochemical[130,131] oxidation, cross-linking of the individual NPs via bi- or trivalent cations,[132–135] polarity or zeta potential changes,[136–138] or via ice-templating.[139–141] In recent years, these techniques have been applied to a variety of NP building blocks made out of different compositions, e.g., semiconductor,[124,128,129,142] metal,[136] semiconductor-metal-hybrid,[143] or magnetic NPs[144,145] as well as out of mixed NP building blocks, e.g., semiconductor and metal NPs,[131,146,147] resulting in a broad range of potential applications in fields like photo-[146,148–151] or electrocatalysis,[140,152–154] (photo)electrochemical sensing,[139,155] or thermoelectrics.[156]

Since the infinite number of achievements in the field of NP-based gel structures[118–120] and the underlying theory[121,122] are widely summarized in literature, within this section, we want to highlight representative examples of nonordered assembled NP-based gels attending to the composition of the NP building blocks, e.g., semiconductor, metal, semiconductor-metal-hybrid, or magnetic NPs, their influence on the properties of the resulting NP-based gel structure as well as their possible and potential applications.

3.1. Semiconductor Building Blocks

Since the pioneering work by Brock et al. in 2004,[124,126] which applied supercritical drying to metal chalcogenide semiconductor NP-based lyogels (**Figure 7**a), reported by Gacion et al. in 1997 first,[125,157] various syntheses for semiconductor NP-based aerogels were developed. These include CdSe,[139,158] CdTe,[137,159] PbTe,[160] ZnS,[161] NP-based aerogels or semiconductor heterostructure NP-based aerogels such as CdSe/ZnS,[162] CdSe/CdS[128,129,132,163] (Figure 7b,c). By controlling the size, shape, facets, and chemical composition of the respective building blocks, the properties of the resulting gel structures can be specifically determined. An example of shape and facet-controlled building blocks for gel structures, already discussed in ordered assemblies, is cadmium chalcogenide-based NPLs. The controlled destabilization of CdSe/CdS core/crown NPLs via chemical oxidation (H_2O_2)[129] or CdSe/CdS and CdSe/CdTe core/crown NPLs via cross-linking with trivalent cations (Y^{3+}, Yb^{3+})[132] leads to interconnected porous gel structures that contain the nanoscopic properties of the NPL building blocks in the macroscopic structure while exhibiting only one type of crystal facet (Figure 7a,b). To avoid the time-consuming and synthesis-intensive wet chemical gelation, CdSe NPLs can also be converted into gel structures by using the cryoaerogelation process. These methods allow the fabrication of CdSe NPL cryoaerogel-coated photoelectrodes for applications in a field like spectroelectrochemistry as well as (photo)electrochemical sensing (Figure 7c).[164]

Furthermore, recent work focuses on the gelation processes and investigations of changes in the (opto)electronic properties of shape and chemical composition-controlled CdSe/CdS dot-in-rod NRs building blocks, which show a quasi-type-II band structure, in which the hole is localized in the core region while
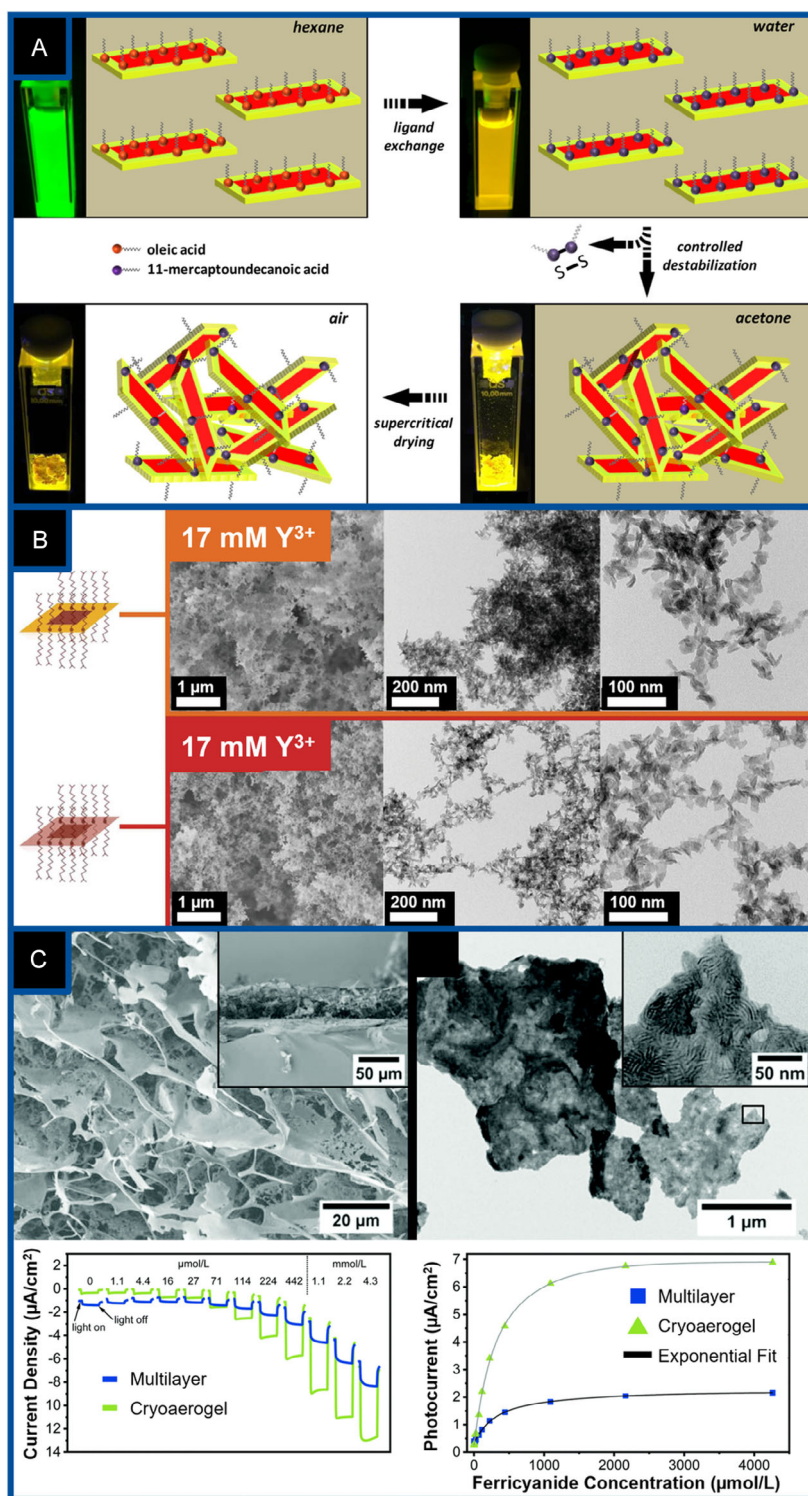
ADVANCED
SCIENCE NEWS

www.advancedsciencenews.com

small
structures

www.small-structures.com

Figure 7. Semiconductor NP-based aerogels with nanoplatelet building blocks. a) Synthesis route for the preparation of luminescent CdSe/CdS core-crown NPL-based aerogels: 1) phase transfer from organic to aqueous medium by ligand exchange, 2) controlled destabilization with H_2O_2, 3) supercritical drying. Insets show photographs of the NPs in solution, in the hydrogel as well as in the aerogel. Adapted with permission.[219] Copyright 2017, American Chemical Society. b) SEM and TEM images of CdSe/CdS (orange) and CdSe/CdTe (red) core-crown NPL-based aerogels prepared by controlled destabilization with trivalent cations (Y^{3+}, Yb^{3+}). Adapted with permission.[220] Copyright 2020, Wiley-VCH Verlag GmbH & Co. KGaA, Weinheim. c) SEM and TEM images of cryoaerogels based on CdSe NPLs (top) and their application in (photo)electrochemical sensing (bottom). The photocurrent responses of a CdSe-NPL multilayer (blue) and a CdSe NPL-coated cryoaerogel photoelectrode (green) on ferricyanide solutions with different concentrations are shown. Adapted with permission.[221] Copyright 2019, Published by the Royal Society of Chemistry.

the electron can be delocalized over the whole NP.[165] Gelation by chemical oxidation (H_2O_2),[128,163] as well as by cross-linking with trivalent cations (Y^{3+}, Yb^{3+})[132] leads to voluminous and porous gel structures, in which the NP building blocks are connected mostly via the tip region. These crystal–crystal contact of the CdSe/CdS NR building blocks allows the band structure to be extended over several NPs, which leads to a stronger charge carrier separation and a significant increase in PL lifetime (PLT) (**Figure 8**a). Theoretical studies have shown that the extension of the PLT in gel structures cannot be attributed to the

delocalization of the electrons in the ground excited state but to electrons in higher excited states (Figure 8b).[166] Since the higher excited states are energetically close to each other, a thermal mixing of these can be assumed, which is in good agreement with the decreased PLT at lower temperatures (Figure 8c).[163] Spectroelectrochemical investigations using intensity-modulated photocurrent spectroscopy (IMPS) confirmed the conductance of the electrons through the gel networks (Figure 8d).[167,168]

As already shown, aerogels based on semiconductor NP exhibit the ability to generate charge carriers by light irradiation,
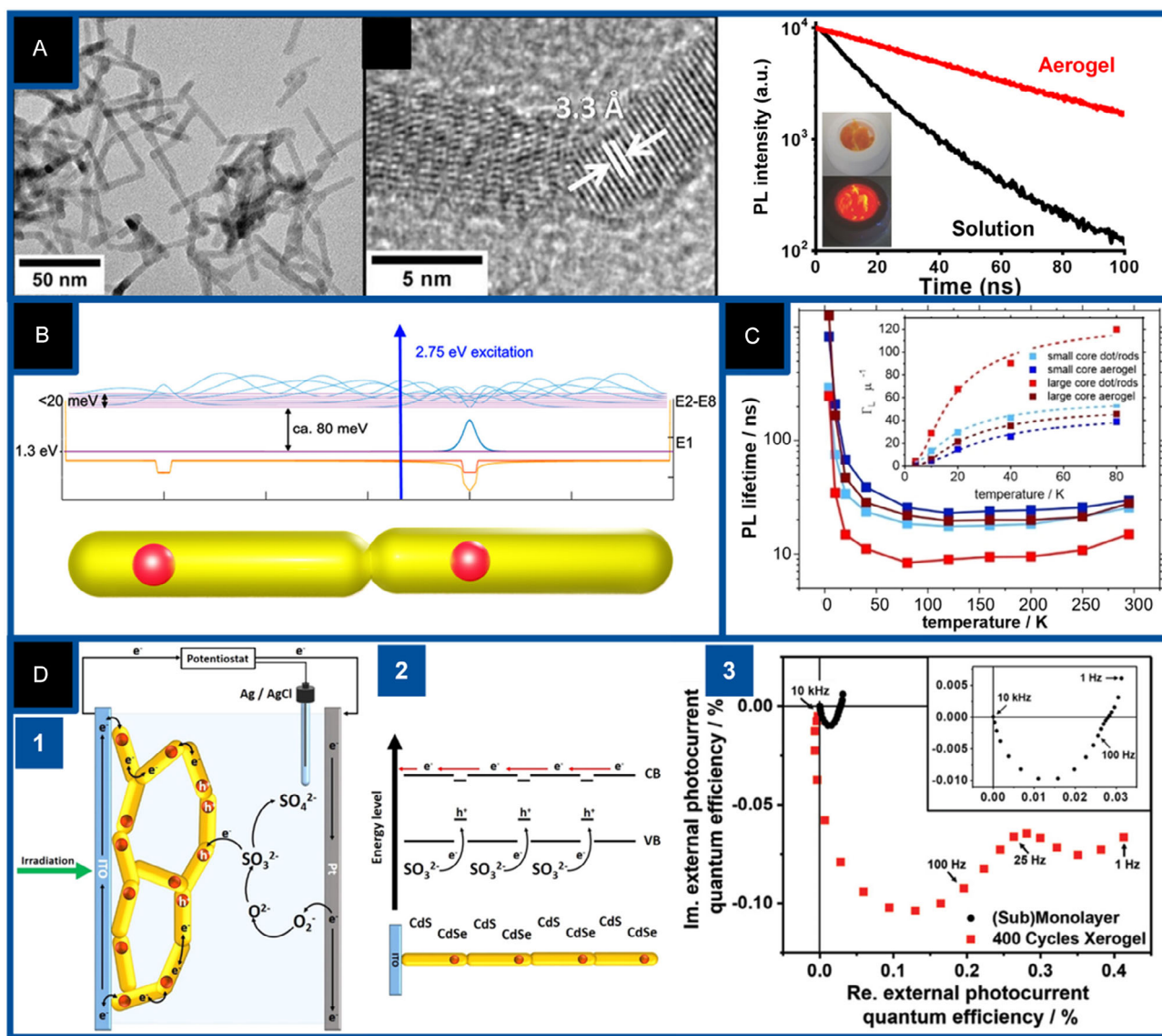

Figure 8. Investigations of the (opto)electronic properties of dot-in-rod shaped CdSe/CdS NR-based gel structures. a) TEM images of tip-to-tip connected CdSe/CdS NR-based aerogels and photoluminescence lifetime measurements showing the increase of lifetime due to particle connection. Adapted with permission.[222] Copyright 2015, Wiley-VCH Verlag GmbH & Co. KGaA, Weinheim. b) Theoretical calculation of the wave function of two tip-to-tip connected CdSe/CdS NRs with delocalization visible for higher excited states. Adapted with permission.[223] Copyright 2019, American Chemical Society. c) Prolongation of photoluminescence lifetimes in CdSe/CdS NR-based gel structures upon reduction of temperature due to thermal mixing of higher excited states. Adapted with permission.[224] Copyright 2021, Wiley-VCH Verlag GmbH & Co. KGaA, Weinheim. d) Schematic representation of the electrochemical processes in CdSe/CdS NR-based gel structures under light irradiation (1) and their diodic behavior (2). IMPS measurements of a CdSe/CdS NR-based gel structure coated electrode showing a charge carrier transport within the network due to the second semicircle at lower frequencies (3). Adapted with permission.[225] Copyright 2019, Wiley-VCH Verlag GmbH & Co. KGaA, Weinheim.

and in combination with their high porosity, they are ideally suited for photocatalysis. In 2017, the Brock group showed that CdS NP-based hydrogels are significantly more efficient than nongelated NP in the photodegradation of organic dyes like methylene blue and methylene orange (**Figure 9**a).[169] In addition, the potential of cadmium chalcogenide-based hydrogels, here CdSe QDs, CdS NRs, and CdSe/CdS NRs, in photocatalytic hydrogen evolution was investigated in our group only recently.

Here, it was shown that the hydrogels show a significantly higher efficiency in hydrogen evolution compared to the nongelated NPs too (Figure 9b).[170] In both examples, the higher efficiency of the gels compared to nongelated NPs can be explained by the gelation process itself as well as the high porosity of the gel structure. To transfer the NP into its gel structure, a ligand exchange with short-chain ligands is carried out beforehand, which shortens the distance from the surrounding medium to the NP surface, thus
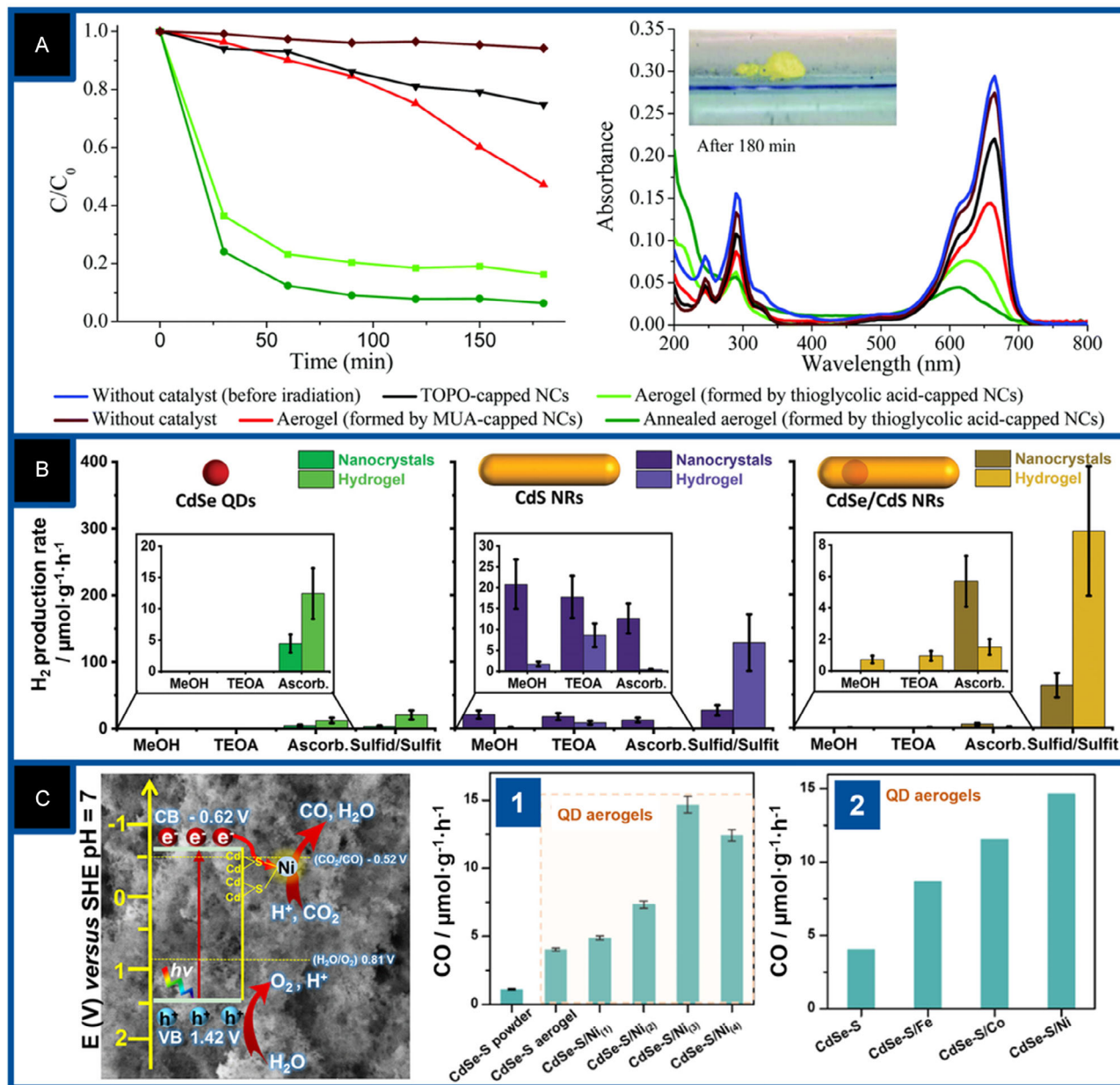

Figure 9. Various examples of semiconductor NP-based gel networks in photocatalysis. a) Photocatalytic degradation of methylene blue using CdS NP-based hydrogels as catalyst (left) and corresponding UV/Vis spectra (right). Adapted with permission.[169] Copyright 2017, Royal Society of Chemistry. b) Photocatalytic hydrogen production with CdSe QD (left), CdS NR (middle), and CdSe/CdS NR-based hydrogels (right) using different hole scavengers, here methanol (MeOH), triethanolamine (TEOA), ascorbic acid (Ascorb.), and a mixture of Na_2S/Na_2SO_3 (Sulfid/Sulfit). Adapted with permission.[170] Copyright 2023, Wiley–VCH Verlag GmbH & Co. KGaA, Weinheim. c) CO_2 photoreduction with CdSe QD-based aerogels and transition-metal cations. 1) Average CO production rates by CdSe-S powders and aerogels with different Ni amounts and 2) different transition metal cations on their surface. Adapted with permission.[171] Copyright 2022, American Chemical Society.

**ADVANCED
SCIENCE NEWS**

www.advancedsciencenews.com

**small
structures**

www.small-structures.com

enabling better charge carrier transfer. Furthermore, the gelation process is based on an oxidation process that removes the ligands from the surface. This results in high, free reactive surfaces where charge carrier transfer from the gel to the reactant can take place. Another interesting example is provided by the Eychmüller group, who have used CdSe QD-based aerogels for CO_2 photoreduction. Here, the combination of CdSe QD-based aerogels with transition-metal cations (Ni, Fe, and Co) as cocatalyst leads to highly efficient catalysts (Figure 9c).[171]

Semiconductor NP-based gels clearly show their potential in photocatalysis. One of the main challenges is to find suitable electron and hole scavengers and cocatalysts for effective photooxidation or photoreduction without destroying the gel network.

3.2. Magnetic Building Blocks

In the field of magnetic nanoparticle-based assemblies, there are only a few works dealing with purely magnetic nanoparticle building blocks and the study of the magnetic properties within the assembly. An example was shown by the Brock group where $Fe_{1.3}Ni_{0.7}P$ rod-shaped NP building blocks were converted to gel structures by chemical oxidation of the surface ligands, here mercaptoundecanoic (MUA) acid and 1-dodecanethiol (DDT). Regardless of the interfaces and the interaction between the NPs, the individual building blocks retain their magnetic properties in the network, which make them interesting for applications in, for example, magnetic refrigeration (**Figure 10**).[172]

Furthermore, many works on magnetic aerogels deal with the incorporation of magnetic NPs into oxides,[173–175] carbons,[176,177] gelatin,[178,179] or polymers,[180] which have already been well summarized in the literature.[181] An interesting example of the incorporation of magnetic NPs into a metal oxide NP-based gel network was shown by the Niederberger group.[173] In addition to the cogelation of TiO_2 and magnetite NPs, the anisotropic assembly of magnetic NPs in a TiO_2 NP-based gel network by applying an external magnetic field was demonstrated. When exposed to a magnetic field, the structured arrangement of the magnetic NPs in the gel network is possible and is reflected in needle-shaped arrangements of the magnetic NPs (**Figure 11**a). In addition, it has been shown by different groups that the incorporation of magnetic iron oxide NPs into graphene-based aerogels leads to materials with interesting applications as well as properties. These multicomponent
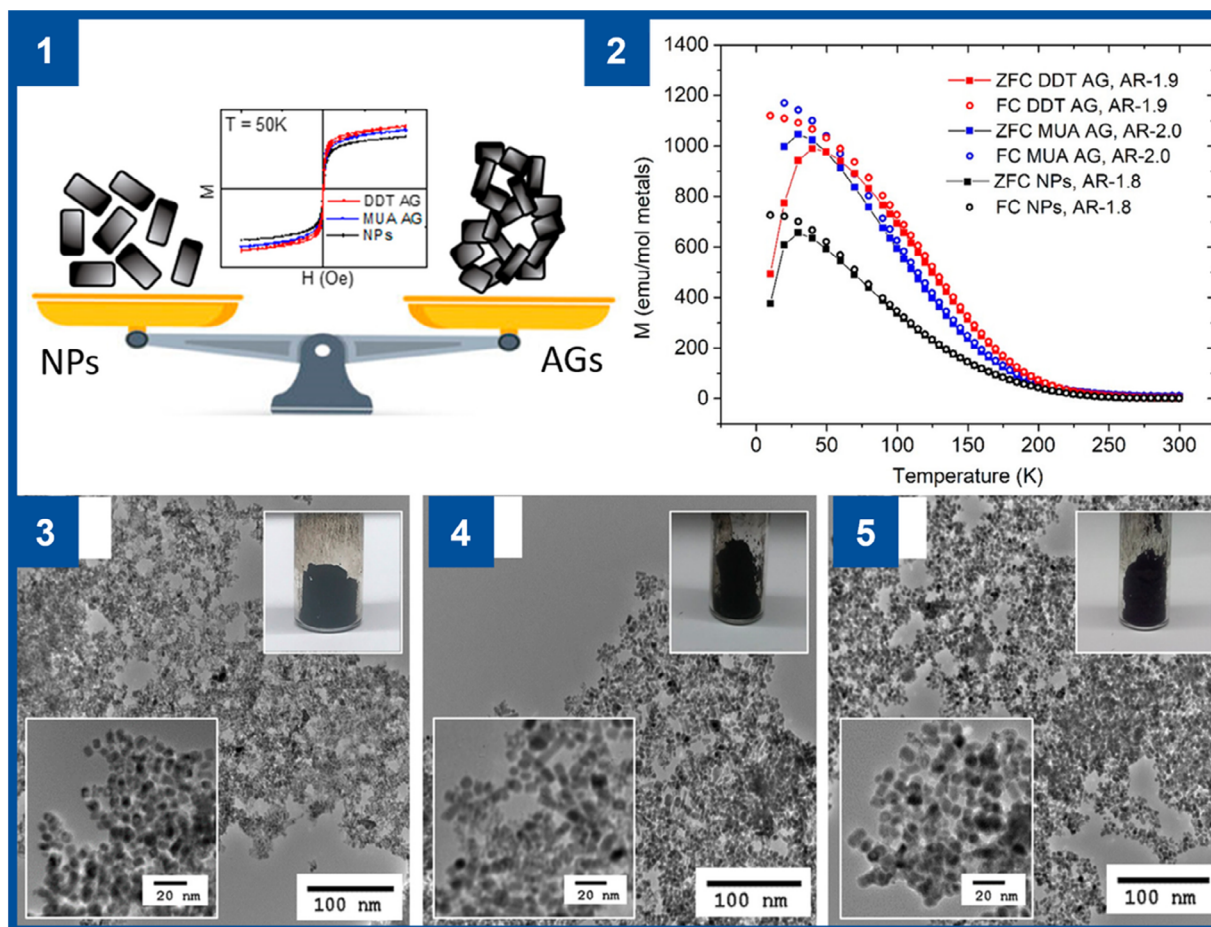

Figure 10. Schematic illustration of NPs and aerogels made of $Fe_{1.3}Ni_{0.7}P$ NP rod-shaped NP building blocks and MH curves (1); ZFC/FC measurements of DDT- and MUA-capped aerogels in comparison to pure NPs (2); photographs and TEM micrographs of $Fe_{1.3}Ni_{0.7}P$ rod-shaped NPs with different aspect ratios (3–5). Adapted with permission.[172] Copyright 2022, American Chemical Society.
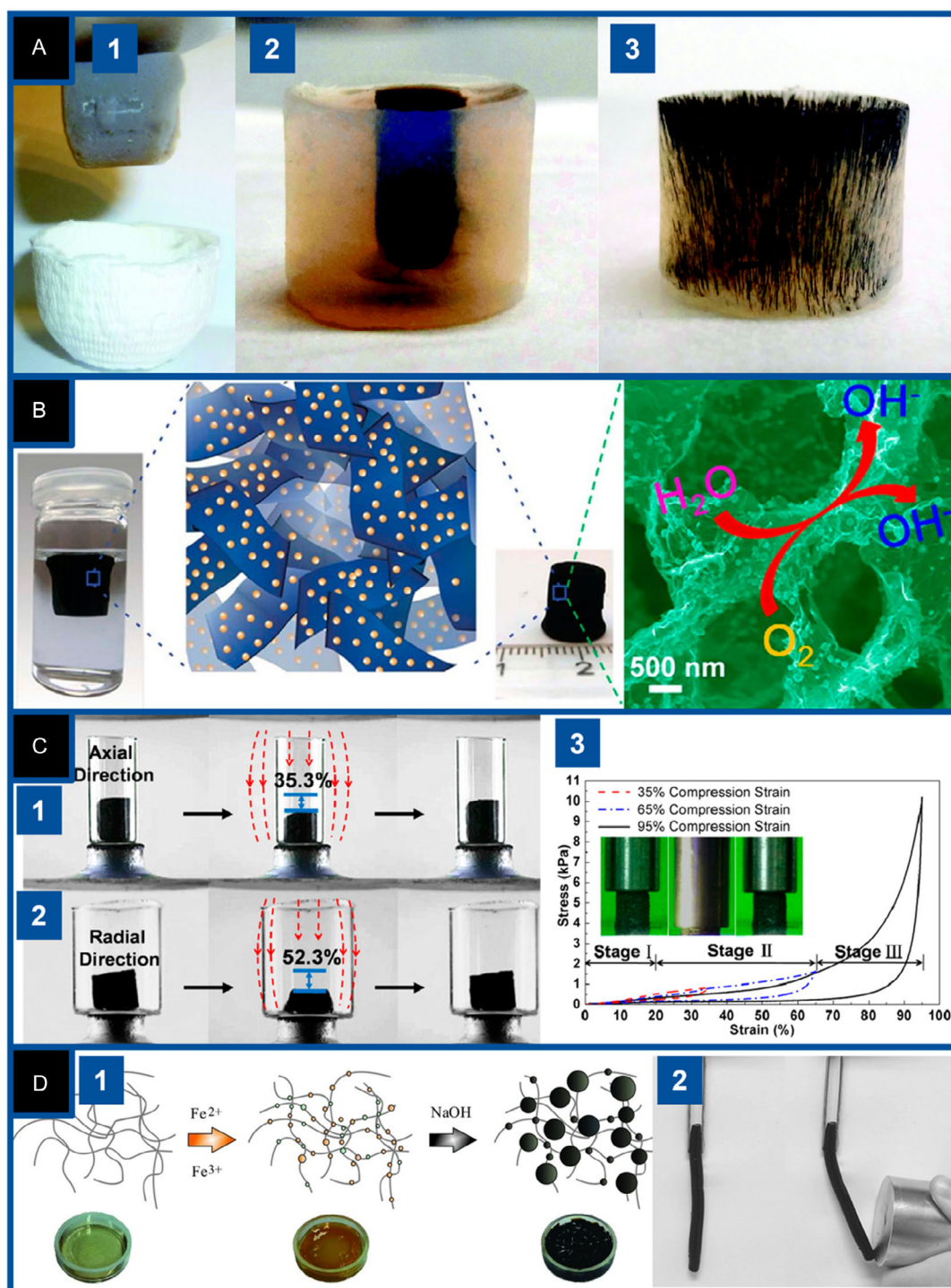
Figure 11. Examples of magnetic multicomponent aerogels. a) Photographs of different TiO_2 and magnetite NP-based gel networks; 1) TiO_2 NP-based gel network with 0.5 mol% Fe_3O_4 NP lifted by a magnet, 2) TiO_2 NP-based gel network with Fe_3O_4 NP core, and 3) TiO_2 NP-based gel network with vertically oriented Fe_3O_4 NPs. Adapted with permission.[173] Copyright 2014, Royal Society of Chemistry. b) Photographs and schematic illustrations of graphene-based gel structure with incorporated Fe_3O_4 NPs for electrocatalysis (oxygen reduction). Adapted with permission.[176] Copyright 2012, American Chemical Society. c) Photographs of graphene-based gel structure with incorporated Fe_3O_4 NPs while magnetic field-induced compression along the axial direction (1) and radial direction (2). Stress–strain curve of graphene-based gel structure with incorporated Fe_3O_4 NPs at maximum strains of 35%, 65%, and 95%, respectively. Adapted with permission.[177] Copyright 2015, American Chemical Society. d) Schematic illustration of the ferrogel synthesis 1) from left to right: unloaded gelatin hydrogel, hydrogel loaded with ferrous and ferric ions, and magnetic NP-loaded gelatin gel. 2) Ferrogel attracted with no magnetic field (left) and external magnetic field (right). Adapted with permission.[178] Copyright 2014, Wiley-VCH Verlag GmbH & Co. KGaA, Weinheim.

**ADVANCED
SCIENCE NEWS**

www.advancedsciencenews.com

**small
structures**

www.small-structures.com

aerogels have been used, for example, in electrocatalysis, such as oxygen reduction (Figure 11b).[176] In addition, these aerogels have been shown to exhibit magnetic field-induced reversible strain of up to 52% and strain-dependent electrical resistance, which can be used to monitor the degree of compression/elongation of the material (Figure 11c).[177] Another interesting variant of embedding magnetic NPs in a gel structure was shown by the Cölfen group.[178,179] In their work, thermoreversible and highly flexible magnetic ferrogels are produced by growing magnetic NPs in situ in a gelatin-based gel network (Figure 11b).

3.3. Metal Building Blocks

Nowadays, porous materials based on metals are indispensable, especially in the field of catalysis. The first work on self-assembly from spherical noble metal nanoparticle building blocks, e.g., Au, Pt, Ag, and mixtures of Ag/Au or Ag/Pt, into a gel structure by using a destabilization agent was reported by the Eychmüller group in 2009 (**Figure 12**a).[182] Thereafter, a variety of different gelation methods were reported, allowing the controlled assembly of metal nanoparticle building blocks into gel structures without the addition of a destabilization agent. One of these variants, so-called one-step approach, is the spontaneous aggregation directly after nanoparticle synthesis. Examples include Pd,[183] Pt,[184] and mixtures of Pd/Pt,[184] PdNi,[185] where the choice of precursor and their mixtures results in the synthesis of metallic and bimetallic NPs, which subsequently assemble into gel structures by spontaneous aggregation (Figure 12b). This gelation method skips time-consuming synthesis steps, such as purification or concentration of the NP solution, and gel structures are obtained in a fast direct way. Regardless of the gelation route, metal NP-based aerogels are ideally suited as electrocatalysts due to their continuous conductivity and ability of material transport, high porosity, and, therefore, high specific surface area.[186] Nowadays, there is a large variety of work dealing with the synthesis of mono-, e.g., Au,[187] Pt,[184,188] Pd,[183] or bimetallic NP-based aerogels, e.g., Au-Pd (Figure 12c),[189] Au-Pt,[190] Pt_xPd_y,[184,191] PdNi,[185,192] PtNi[193,194] (Figure 12d) and their application in electrocatalytic reactions, e.g., ethanol oxidation reaction (EOR), CO_2-reduction reaction (CO_2RR) (Figure 12e),[189,191,195] ORR,[184] and many more. High electrocatalytic performance is shown, for example, by measuring cyclic voltammetry and chronoamperometric of cyclodextrin-modified Pd (Pd_{CD}) aerogels. Compared to commercially available catalysts Pd/C (10 wt%), the aerogels show significantly higher mass-specific current densities and enhanced kinetics in EOR (Figure 12f).

Another variant for the preparation of metal NP-based gel networks without the addition of a destabilization agent is the cryoaerogelation process (which is also possible for other nonmetallic nanocrystal building blocks but will be introduced here).[37,141,154,196–199] By this route, aqueous and highly concentrated Ag, Au, Pd, and Pt NP solutions are converted into monolithic cryohydrogels by flash freezing with, e.g., liquid nitrogen (**Figure 13**a).[141] The driving force for the formation of the monolithic structure is the formation of ice crystals, while the building blocks are pressed in the space between the ice crystallites, finally obtaining sheet-like structures. The cryoaerogelation has the great advantage that, by using templates, defined monolithic structures can be created (Figure 13a). This advantage has been exploited in further work by our group to develop additive-free and self-assembled Au, Pt, and Pd NP-based gel network-coated electrodes for application in electrocatalysis.[154] In addition to defined coated areas, the electrodes exhibit high porosity and good surface accessibility as well as the adjustability of the coated area size; the morphology of the obtained electrodes could be influenced by the choice of the freezing medium, e.g., liquid nitrogen, n-hexane, toluene, n-pentane, isopentane, and consequently the freezing temperature (Figure 13b).[196] These metal NP-based cryoaerogel-coated electrodes are also used as an electrocatalyst, which shows improved electrocatalytic activity in EOR compared to their dried NP films. It is interesting to note that the freezing to cryohydrogel already leads to effective gel structure and that the time-consuming lyophilization to produce the cryoaerogel structure is not absolutely necessary (Figure 13c).[154] In addition to spherical noble-metal NPs, it was also shown that shaped, controlled Au and Ag NRs can be used as building blocks for cryoaerogel-coated electrodes leading to different electrocatalytic results in EOR depending on the material. Au NR-based cryoaerogels were shown to exhibit high activity in EOR compared to pure dropcasted NP-based electrodes, but neither Ag NR-based cryoaerogels nor pure dropcasted NP-based electrodes exhibited activity, which indicated that either the crystal facets of the Ag NRs are not active in this catalytic reaction, or the NRs lose their active facets due to their instability in alkaline medium (Figure 13d).

3.4. Hybrid Building Blocks

The functionality and range of application of gel structures can be greatly varied by the composition of the NP building blocks as well as their chemical composition. Even the mixing of different NPs, such as semiconductors and metals, leads to altered optical properties as well as charge carrier movements in the network. Initial work by the Eychmüller group on mixtures of semiconductor chalcogenide CdTe and Au NPs has shown that regardless of the gelation method (cross-linking with ions (**Figure 14**a)[200] or photooxidation of the ligands (Figure 14b)[201]), hybrid gel networks can be obtained in which the optical properties, such as PL or PL lifetime, are quenched or significantly shortened by increasing the Au content (Figure 14b).[200,201] A work investigating the influence of quenching properties of gold NPs on photoluminescent semiconductor gel structures, here CdSe/CdS NR-based, more in detail, was carried out by our group. Through optical characterizations and calculations, it was shown that one gold nanoparticle could quench up to nine NRs in the near vicinity (Figure 14c).[147] In addition, it could be shown in further work that the use of different bivalent (Ca^{2+}, Ba^{2+}) or trivalent (Yb^{3+}, Y^{3+}) cations in the gelation process of mixtures of CdSe/CdS NR and Au NP lead to differently connected gel networks (Figure 14d).

Hybrid nanoparticle building blocks, e.g., metal-semiconductor NPs like CdS-Ag (**Figure 15**a),[202] CdSe/CdS-Au (Figure 15b),[199,203] CdSe/CdS-Pt (Figure 15c),[203] offer an alternative to mixing individual nanoparticle building blocks for the fabrication of multicomponent gel structures. A grown
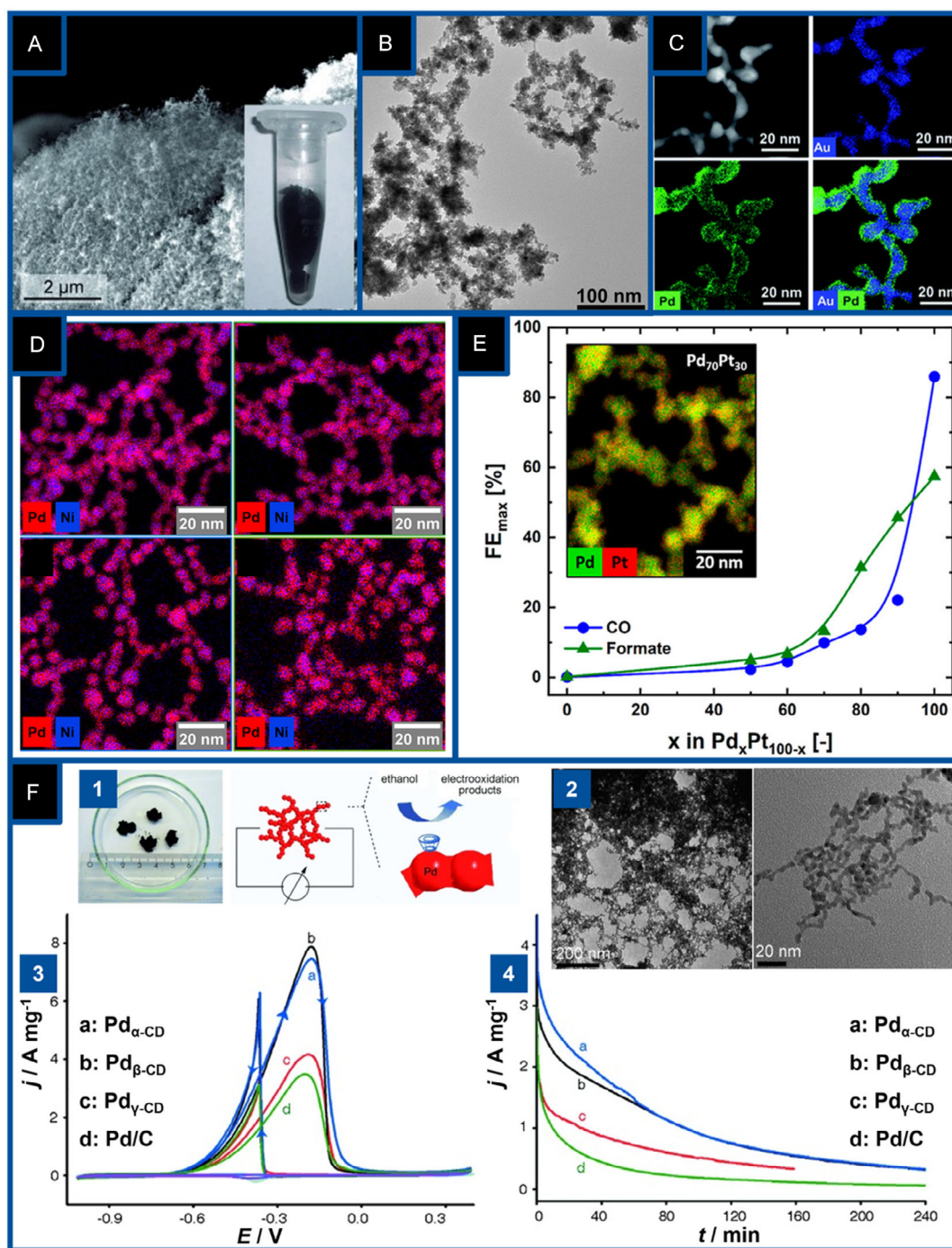
Figure 12. Examples of gel structures based on noble metal NP and bimetallic NPs synthesized using different gelation methods and its application in electrocatalysis. a) SEM image of a self-supporting Pt NP-based aerogel synthesized by adding a destabilization agent. The inset shows a photograph of a monolithic Pt NP-based hydrogel. Adapted with permission.[182] Copyright 2009, Wiley–VCH Verlag GmbH & Co. KGaA, Weinheim. b) TEM images of $Pd_{83}Ni_{17}$ NP-based aerogels synthesized without the addition of any destabilization agent. Adapted with permission.[185] Copyright 2014, Wiley–VCH Verlag GmbH & Co. KGaA, Weinheim. c) HAADF-STEM image and corresponding EDX-mappings of core–shell Au-Pd aerogel. Adapted with permission.[189] Copyright 2021, Royal Society of Chemistry. d) EDX-based elemental distribution of Pd (red) and Ni (blue) of 2D Pt-Ni aerogels. Adapted with permission.[194] Copyright 2023, American Chemical Society. e) Maximum FE toward CO and formate production as a function of Pd content in the aerogel and as an inset the EDX-based elemental distribution of Pd (green) and Pt (red) of the PdPt aerogel. Adapted with permission.[226] Copyright 2022, American Chemical Society. f) (1) Photographs and illustration of the electrocatalytic performance of cyclodextrin-modified Pd aerogel in EOR and (2) TEM images in different magnifications. (3) Cyclic voltammograms (CV) of electrodes different modified electrodes in 0.1 M KOH + 1.0 M C_2H_5OH with a scan rate of 50 mV s^{-1} and (4) chronoamperometric curves for ethanol electrooxidation at −0.3 V in 0.1 M KOH + 1.0 M C_2H_5OH. Adapted with permission.[183] Copyright 2012, Wiley–VCH Verlag GmbH & Co. KGaA, Weinheim.
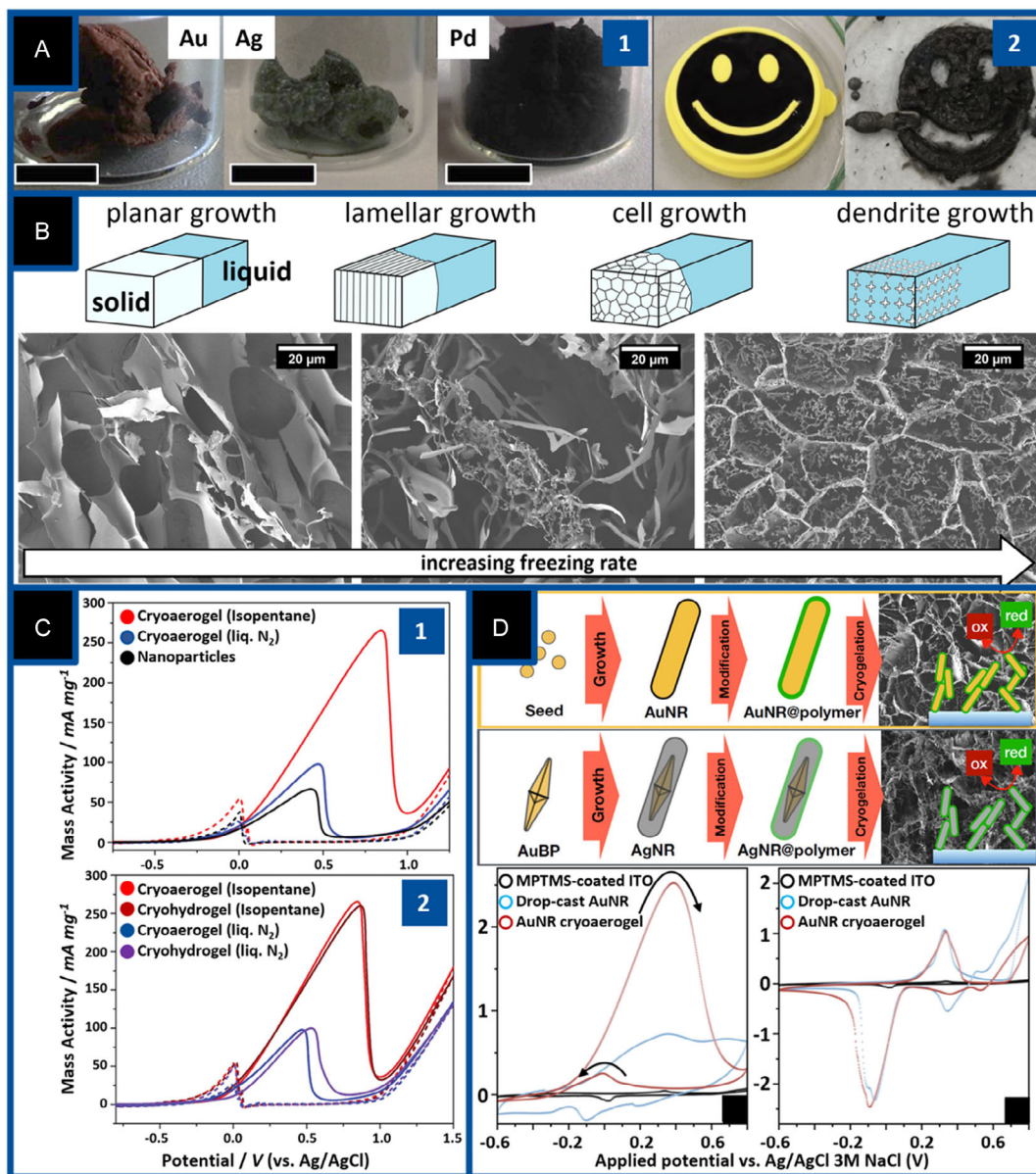
Figure 13. Cryoaerogels achieved by cryogelation method. a) Photographs of monolithic cryoaerogels based on Au, Ag, and Pd NPs (1) and template-supported production of a cryoaerogel in the form of a 3D smile (2). (2, left) liquid NP solution in the template and (2, right) freeze-dried cryoaerogel in the form of the 3D smile. Adapted with permission.[141] Copyright 2015, Wiley–VCH Verlag GmbH & Co. KGaA, Weinheim. b) Variation of the morphologies of the cryoaerogels by freezing with different freezing media with the corresponding SEM images (left: n-hexane, middle: pentane, right: isopentane). Adapted with permission.[196] Copyright 2021, American Chemical Society. c) Mass-normalized cyclic voltammogram of various gold coatings (1) and gold NP-based cryohydrogels and cryoaerogels in N_2-saturated KOH solution (1 M) containing ethanol (1 M) at a scan rate of 50 mV s^{-1}. Adapted with permission.[154] Copyright 2021, Wiley-VCH Verlag GmbH & Co. KGaA, Weinheim. d) Schematic illustration of Au and Ag noble-metal NR-based cryoaerogels with electrocatalytically active surface sites and their application in EOR (1 M EtOh in 0.3 M KOH). Adapted with permission.[197] Copyright 2021, American Chemical Society.

metal domain on a semiconductor allows rapid charge carrier separation of the excited electron and hole and enables application in redox reactions. Initial studies have shown that the use of CdSe/CdS-Au metal-semiconductor hybrid nanoparticle building blocks for gelation lead to gel structures with enhanced charge carrier mobility. By spectroelectrochemical investigations such as linear sweep voltammetry or IMPS, the effective charge

carrier separation and the accumulation of electrons in the metal domain could be demonstrated (Figure 15b).[199] In another study, it was shown that the charge carrier separation in cryoaerogel-coated electrodes made of mixtures of semiconductor and metal NPs is more difficult or slower than in cryoaerogel-coated electrodes made of hybrid metal-semiconductor NPs. One reason for this is the contact or connection of the NP to each
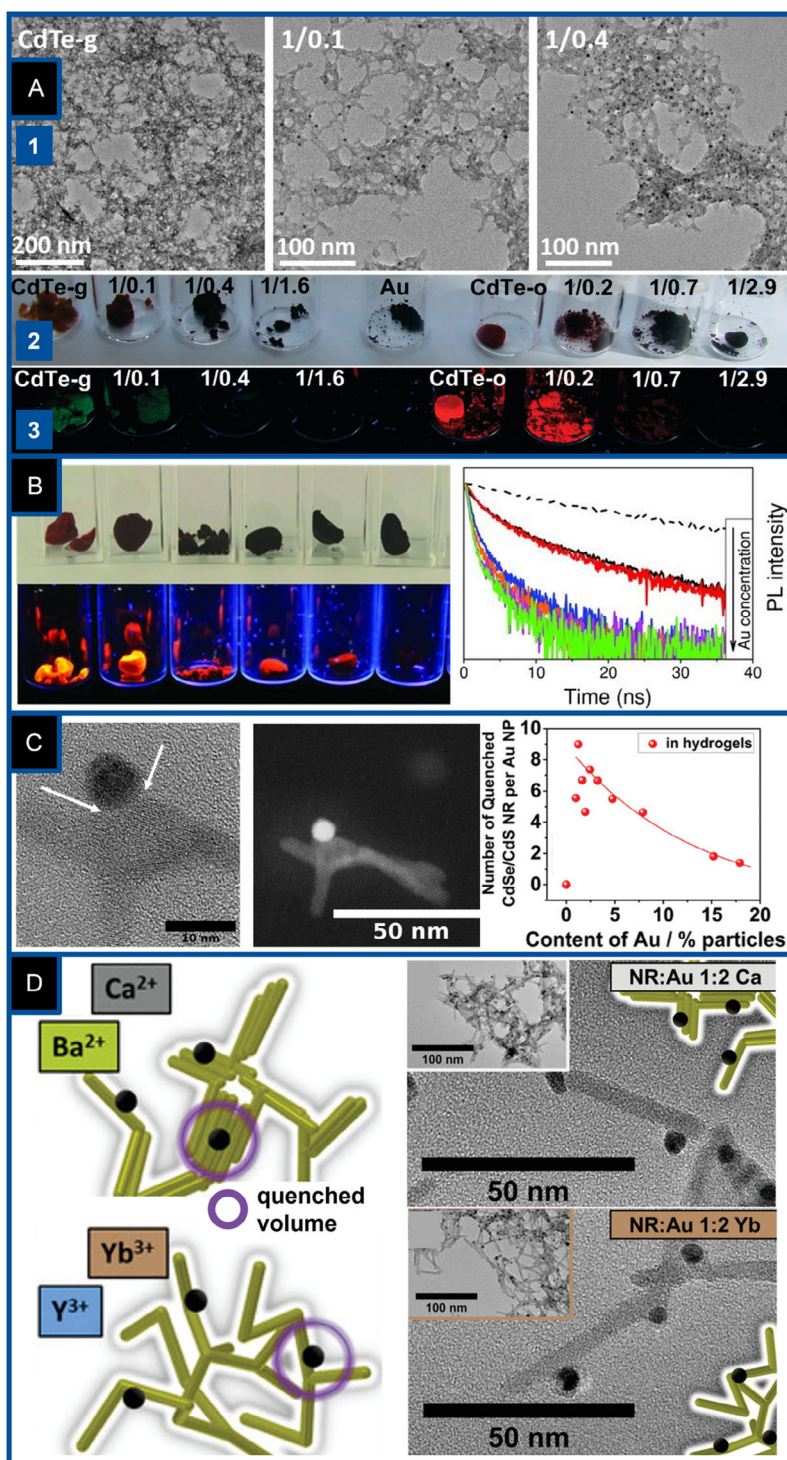
Figure 14. Aerogels consisting of mixtures of metal and semiconductor nanoparticle building blocks and characterization of the modified optical properties. a) TEM images (1) and photographs under daylight irradiation (2) and UV light excitation (3) of cogelated CdTe QDs and Au NPs via ionic linking. Adapted with permission.[200] Copyright 2011, American Chemical Society. b) Photographs (left) and photoluminescence lifetime measurements (right) of a mixed aerogel of CdTe and Au NP. With increasing gold content, the photoluminescence is quenched, and thus, the photoluminescence lifetime is shortened. Adapted with permission.[201] Copyright 2013, WILEY–VCH Verlag GmbH & Co. KGaA, Weinheim. c) Mixed aerogels of CdSe/CdS NRs and Au NPs gelated via chemical oxidation with H_2O_2. The calculated number of quenched CdSe/CdS NRs with change of Au content (left) and HR-TEM and STEM-HAADF images of a selected area showing a CdSe/CdS NR and Au NP contact (right). Adapted with permission.[147] Copyright 2021, WILEY-VCH Verlag GmbH & Co. KGaA, Weinheim. d) Schematic illustration (left) and TEM micrographs of mixed aerogels of CdSe/CdS NRs and Au NPs gelated by the addition of bi- and trivalent cations. Adapted with permission.[227] Copyright 2023, WILEY-VCH Verlag GmbH & Co. KGaA, Weinheim.

**ADVANCED
SCIENCE NEWS**

www.advancedsciencenews.com
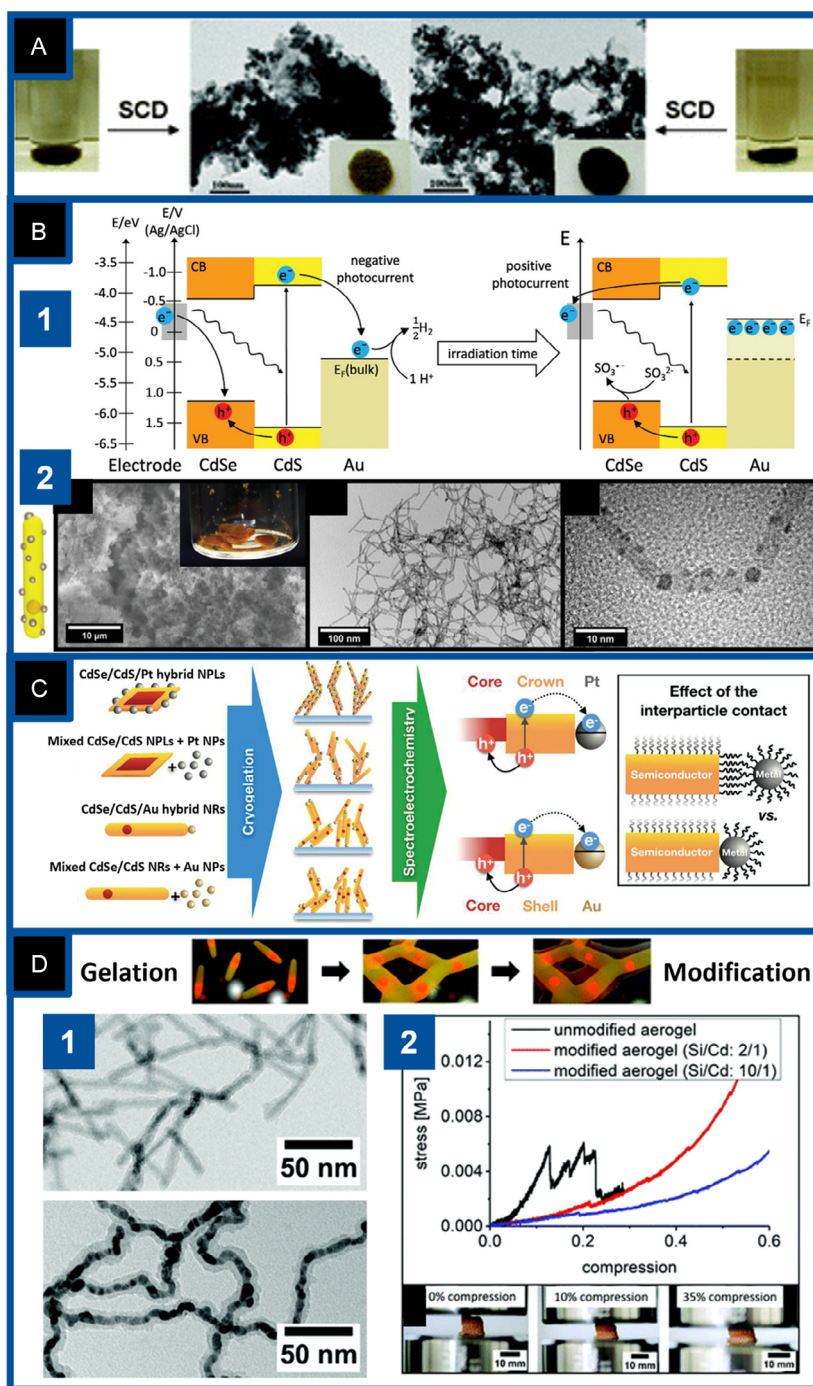
**small
structures**

www.small-structures.com

Figure 15. Example of gel structures based on metal-semiconductor hybrid NPs and (spectro)electrochemical studies on various aerogels and cryoaerogel-coated electrodes based on metal-semiconductor hybrid NPs and mixtures of metal and semiconductor NPs. a) Photographs and TEM images of CdS-Ag hybrid NP-based gel structures. Adapted with permission.[202] Copyright 2009, Royal Society of Chemistry. b) Scheme of the energy landscape of CdSe/CdS-Au hybrid heteronanoparticle showing the electron accumulation and the increase of the Fermi level in the metal domain with longer irradiation time and the subsequent change of the photocurrent direction (1). SEM and TEM micrographs (2) show aerogel structures consisting of random-decorated CdSe/CdS-Au NPs. Adapted with permission.[199] Copyright 2021, Wiley–VCH Verlag GmbH & Co. KGaA, Weinheim. c) Schematic illustration of investigated cryoaaerogel-coated electrode systems made of different semiconductor (NPLs or NRs) and metal (Pt or Au) nanoparticle building blocks. The metal nanoparticle building blocks are either grown directly on the semiconductor or mixed with the semiconductors as individual NPs. Adapted with permission.[203] Copyright 2022, Wiley–VCH Verlag GmbH & Co. KGaA, Weinheim. d) Scheme two-step process of gelation and post-modification. 1) TEM images of CdSe/CdS NR-based (top) and Au and Ag NP-based (down) gel structure covered with a silica shell. 2) Mechanical measurement of unmodified and silica shell-modified CdSe/CdS NR-based gel structures by compression tests and photographs showing silica shell-modified gel structure at various points of the measurement. Adapted with permission.[204] Copyright 2019, Royal Society of Chemistry.

**ADVANCED
SCIENCE NEWS**

www.advancedsciencenews.com

**small
structures**

www.small-structures.com

other within the different networks. In cryoaerogels consisting of mixtures of two nanoparticle types, there is a defined distance between the building block due to the ligand shell of the respective NPs. This distance has to be overcome during the charge carrier transfer. If, on the other hand, the metal domain is grown directly onto the semiconductor, this distance does not exist, and the charge carrier transfer can take place without overcoming a barrier (Figure 15c).[203]
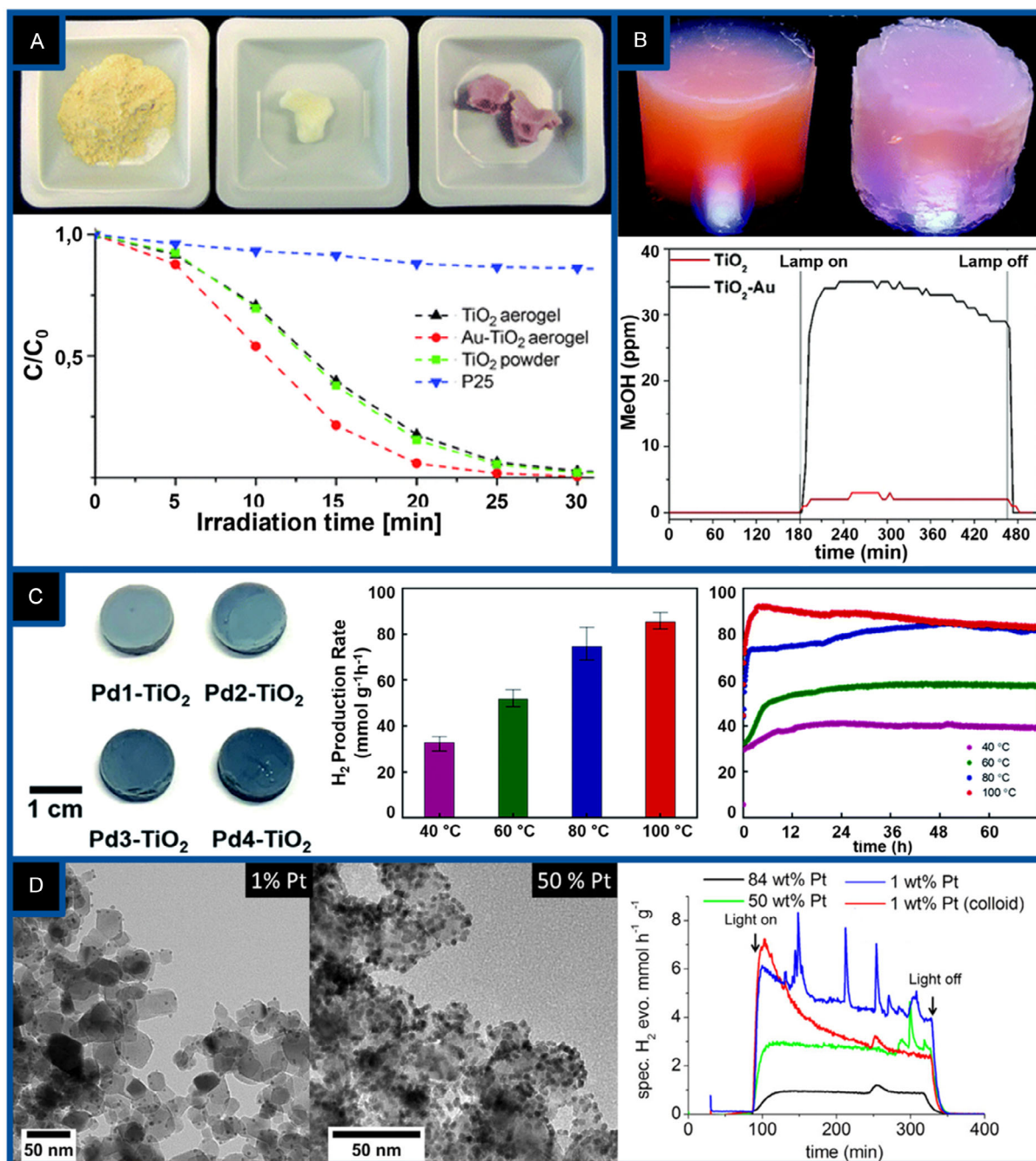

Figure 16. Examples of aerogels based on cogelated TiO_2 and metal NPs and hybrid TiO_2-metal NP for application in photoinduced reactions. a) Photographs of TiO_2 NP powder, TiO_2 NP-based aerogel, and TiO_2 and Au NP-based aerogels as well as the photodegradation of Rhodamine B investigated at the different samples. Adapted with permission.[205] Copyright 2011, Royal Society of Chemistry. b) Photographs of TiO_2 and Au NP-based aerogel before (left) and after (right) photoreduction reaction with CO_2 as well as photocatalytic reduction of CO_2 on TiO_2 and TiO_2-Au multicomponent aerogel. Adapted with permission.[206] Copyright 2017, Royal Society of Chemistry. c) Photographs of TiO_2-Pd hybrid NP-based aerogels with different Pd content (right) and visible-light-induced photocatalytic H_2 production rate (middle) and stability test measurements (right). Adapted with permission.[207] Copyright 2022, Royal Society of Chemistry. d) TEM images of cryoaoergels based on TiO_2 and Pt NPs (left) and light-induced photocatalytic H_2 production (right). Adapted with permission.[198] Copyright 2018, American Chemical Society.

Furthermore, an interesting variant to synthesize multicomponent aerogels with significantly increased mechanical stability is the post-modification by shell growth, e.g., SiO_2, TiO_2, around the existing gel structure, e.g., CdSe/CdS NR-based, Au, and Ag NPs.[204] The growth of a continuous shell has the advantage of mechanically reinforcing the gel structure (Figure 15d), and depending on the material used, it can provide an isolating barrier for charge carrier transfer, e.g., SiO_2, or support charge transfer when using, for example, semiconducting or metallic materials.

In addition to chalcogenide semiconductors, semiconductors based on metal oxides like TiO_2 are also used in cogelated aerogel structures for redox reactions, photodegradation,[205] or photocatalysis.[198,206,207] In a first study, the Niederberger group was able to show that compared to a pure TiO_2 NP-based aerogel, an aerogel consisting of a mixture of TiO_2 and Au NPs exhibited a significantly higher efficiency in light-induced reactions, here the photodegradation of Rhodamine B (**Figure 16**a).[205] Interestingly, further studies show that this system can be applied to convert CO_2 and water to methanol in a gas phase reaction under the irradiation of sunlight. By using the system, two problems can be addressed; one is the reduction of CO_2 in the atmosphere, and the other is the production of fossil fuels such as methane and methanol (Figure 16b).[206] Besides Au, Pt and Pd are also used in the mixed structures, which show application in the field of photocatalysis and hydrogen evolution.[198,207] For example, it has been shown that aerogels based on TiO_2 NPs covered with on-grown Pd domains (Figure 16c),[207] as well as cryoaerogels based on mixtures of TiO_2 and Pt NPs, exhibit high hydrogen evolution efficiencies (Figure 16d).[198]

3.5. Summary and Outlook Nonordered Assemblies

Nonordered assemblies based on well-defined NP building blocks allow the fabrication of macroscopic and monolithic structures in which the nanoscopic properties of the individual NP building blocks are retained. In addition, the macroscopic nonordered assemblies exhibit high porosity and reactive surface area. Depending on the materials, e.g., semiconducting, metallic, magnetic, or material compositions, e.g., metal-semiconductor hybrids used, the NP-based gel networks can be specifically fabricated for the desired application. For example, as shown earlier, semiconductor NP-based gels are ideally suited for photocatalysis or sensing due to their ability to generate charge carriers by light irradiation. Combining this capability with the high porosity and free reactive surface makes them highly efficient photocatalysts compared to pure NP.[169–171] Generally, to achieve the maximum efficiency in photooxidation or photoreduction, the right choice of the appropriate hole or electron scavenger, or cocatalyst is crucial.[208,209] Numerous works on pure NPs are known in the literature,[210–212] which can be the basis and inspiration to develop highly efficient photocatalysts based on semiconductor NP-based gel networks. In addition to photocatalysis and as discussed above, metal NP-based gel networks are currently being used in the field of electrocatalysis.

Regardless of the material and application, fragility and handling remain one of the main challenges in dealing with NP-based gel networks. Initial solutions include immobilization of the gel networks on substrates[213,214] or mechanical reinforcement of the gel networks with an inorganic shell.[215,216] Mechanical reinforcement can be done before or after gelation, obtaining gels with higher stability and different properties. Furthermore, as has been shown, different building blocks can be used to obtain gel structures, and it is also possible to fabricate hybrid systems where postgelation cation exchange is possible. The goal is to provide these structures with new functionalities, e.g., by further advancing stimuli-responsive gelation or by obtaining reversible gels.

4. Summary

The assembly of inorganic NPs gives place to a myriad of new functional materials with properties that can go beyond the individual properties of the building blocks as well as their collective expected behavior. These materials are possible due to the efforts done in colloidal synthesis and advances in nanochemistry, allowing to design of high-quality macroscopic objects with novel and tailored properties.

As can be seen in the examples discussed earlier, the building blocks can arrange in well-organized 1D, 2D, or 3D structures, whose assembly can be assisted by external fields or in nonordered networks by destabilizing the colloidal NP solutions. Moreover, the possibility of using NPs with different compositions and shapes, as well as mixtures of them, in addition to their structure itself, opens the door to a complete, fascinating toolbox of materials with plenty of applications, such as electro- and photocatalysis, sensing, optoelectronics, magnetofection, drug delivery, and many others, some of which will appear in the following years as knowledge about these structures and their properties increases.

Conflict of Interest

The authors declare no conflict of interest.

Keywords

[1] A. L. Efros, L. E. Brus, *ACS Nano* **2021**, *15*, 6192.

[2] F. Montanarella, M. V. Kovalenko, *ACS Nano* **2022**, *16*, 5085.

[3] K. D. Gilroy, A. Ruditskiy, H.-C. Peng, D. Qin, Y. Xia, *Chem. Rev.* **2016**, *116*, 10414.

[4] L. Wu, A. Mendoza-Garcia, Q. Li, S. Sun, *Chem. Rev.* **2016**, *116*, 10473.

[5] L. De Trizio, L. Manna, *Chem. Rev.* **2016**, *116*, 10852.

[6] M. Nasilowski, B. Mahler, E. Lhuillier, S. Ithurria, B. Dubertret, *Chem. Rev.* **2016**, *116*, 10934.

[7] G. M. Whitesides, B. Grzybowski, *Science* **2002**, *295*, 2418.

[8] D. V. Talapin, M. Engel, P. V. Braun, *MRS. Bull.* **2020**, *45*, 799.

[9] T. Bian, A. Gardin, J. Gemen, L. Houben, C. Perego, B. Lee, N. Elad, Z. Chu, G. M. Pavan, R. Klajn, *Nat. Chem.* **2021**, *13*, 940.

[10] A. Arango-Restrepo, D. Barragán, J. M. Rubi, *Phys. Chem. Chem. Phys.* **2019**, *21*, 17475.

[11] Z. Nie, A. Petukhova, E. Kumacheva, *Nat. Nanotechnol.* **2009**, *5*, 15.

[12] S. Förster, M. Konrad, *J. Mater. Chem.* **2003**, *13*, 2671.

[13] Y. Zhou, D. Yan, *Chem. Commun.* **2009**, *1172*.

[14] C. Li, Q. Li, Y. V. Kaneti, D. Hou, Y. Yamauchi, Y. Mai, *Chem. Soc. Rev.* **2020**, *49*, 4681.

[15] C. K. Wong, X. Qiang, A. H. E. Müller, A. H. Gröschel, *Prog. Polym. Sci.* **2020**, *102*, 101211.

[16] M. A. Boles, M. Engel, D. V. Talapin, *Chem. Rev.* **2016**, *116*, 11220.

[17] X. Li, X. Liu, X. Liu, *Chem. Soc. Rev.* **2021**, *50*, 2074.

[18] Z. Lin Wang, Y. Lui, Z. Zhang, in *Handbook of Nanophase and Nanostructured Materials*, Kluwer Academic/Plenum Publishers, Amsterdam **2003**, p. 1297.

[19] H. Cölfen, S. Mann, *Angew. Chem. Int. Ed.* **2003**, *42*, 2350.

[20] W. Wei, S. Ouyang, T. Zhang, Z. Yong-Jun, Y. Jing-Hai, W. Li, V. Amadi, A. Venkataraman, C. Papadopoulos, *Nanotechnology* **2022**, *33*, 132001.

[21] R. Thiruvengadathan, V. Korampally, A. Ghosh, N. Chanda, K. Gangopadhyay, S. Gangopadhyay, *Rep. Progr. Phys.* **2013**, *76*, 066501.

[22] T. Wang, D. La Montagne, J. Lynch, J. Zhuang, Y. C. Cao, *Chem. Soc. Rev.* **2013**, *42*, 2804.

[23] S. Ithurria, B. Dubertret, *J. Am. Chem. Soc.* **2008**, *130*, 16504.

[24] A. E. Saunders, A. Ghezelbash, D.-M. Smilgies, M. B. Sigman, B. A. Korgel, *Nano. Lett.* **2006**, *6*, 2959.

[25] X.-S. Du, M. Mo, R. Zheng, S.-H. Lim, Y. Meng, Y.-W. Mai, *Cryst. Growth. Des.* **2008**, *8*, 2032.

[26] T. G. Mason, *Phys. Rev. E* **2002**, *66*, 60402.

[27] A. Antanovich, A. Prudnikau, A. Matsukovich, A. Achtstein, M. Artemyev, B. I. Stepanov, *J. Phys. Chem. C* **2016**, *120*, 29.

[28] M. Li, H. Schnablegger, S. Mann, *Nature* **1999**, *402*, 393.

[29] I. Dozov, C. Goldmann, P. Davidson, B. Abécassis, *Nanoscale* **2020**, *12*, 11040.

[30] M. D. Tessier, L. Biadala, C. Bouet, S. Ithurria, B. Abecassis, B. Dubertret, *ACS. Nano* **2013**, *7*, 3332.

[31] S. Jana, M. De Frutos, P. Davidson, B. Abécassis, *Sci. Adv.* **2017**, *3*, 1701483.

[32] S. Jana, T. N. T. Phan, C. Bouet, M. D. Tessier, P. Davidson, B. Dubertret, B. Abécassis, *Langmuir* **2015**, *31*, 10532.

[33] L. Guillemeney, L. Lermusiaux, G. Landaburu, B. Wagnon, B. Abécassis, *Commun. Chem.* **2022**, *5*, 1.

[34] R. Momper, H. Zhang, S. Chen, H. Halim, E. Johannes, S. Yordanov, D. Braga, B. Blu, D. Doblas, T. Kraus, M. Bonn, H. I. Wang, A. Riedinger, *Nano Lett.* **2020**, *20*, 4102.

[35] B. Abécassis, M. D. Tessier, P. Davidson, B. Dubertret, *Nano Lett.* **2014**, *14*, 710.

[36] B. Guzelturk, O. Erdem, M. Olutas, Y. Kelestemur, H. V. Demir, *ACS Nano* **2014**, *8*, 12524.

[37] A. Schlosser, L. C. Meyer, F. Lübkemann, J. F. Miethe, N. C. Bigall, *Phys. Chem. Chem. Phys.* **2019**, *21*, 9002.

[38] R. T. Graf, A. Schlosser, D. Zámbó, J. Schlenkrich, P. Rusch, A. Chatterjee, H. Pfnür, N. C. Bigall, *Adv. Funct. Mater.* **2022**, 2112621.

[39] J. F. Miethe, A. Schlosser, J. G. Eckert, F. Lübkemann, N. C. Bigall, *J. Mater. Chem. C Mater.* **2018**, *6*, 10916.

[40] M. Micheel, R. Baruah, K. Kumar, M. Wächtler, M. Micheel, R. Baruah, K. Kumar, M. Wächtler, *Adv. Mater. Interfaces* **2022**, *9*, 2201039.

[41] O. Erdem, S. Foroutan, N. Gheshlaghi, B. Guzelturk, Y. Altintas, H. V. Demir, *Nano Lett.* **2020**, *20*, 6459.

[42] Y. Gao, M. C. Weidman, W. A. Tisdale, *Nano Lett.* **2017**, *17*, 3837.

[43] R. Momper, H. Zhang, S. Chen, H. Halim, E. Johannes, S. Yordanov, D. Braga, B. Blülle, D. Doblas, T. Kraus, T. Kraus, M. Bonn, H. I. Wang, A. Riedinger, *Nano Lett.* **2020**, *20*, 4102.

[44] O. Erdem, K. Gungor, B. Guzelturk, I. Tanriover, M. Sak, M. Olutas, D. Dede, Y. Kelestemur, H. V. Demir, *Nano Lett* **2019**, *19*, 4297.

[45] J. Liu, L. Guillemeney, L. Abécassis, L. Coolen, *Nano Lett* **2020**, *20*, 3465.

[46] L. Guillemeney, L. Lermusiaux, G. Landaburu, B. Wagnon, B. Abécassis, *Commun. Chem.* **2022**, *5*, 1.

[47] W. D. Kim, D.-E. Yoon, D. Kim, S. Koh, W. K. Bae, W.-S. Chae, D. C. Lee, *J. Phys. Chem. C* **2019**, *123*, 15.

[48] J. Yan, W. Feng, J. Y. Kim, J. Lu, P. Kumar, Z. Mu, X. Wu, X. Mao, N. A. Kotov, *Chem. Mater.* **2020**, *32*, 476.

[49] J. Lv, X. Gao, B. Han, Y. Zhu, K. Hou, Z. Tang, *Nat. Rev. Chem.* **2022**, *6*, 125.

[50] T. Wang, J. Zhuang, J. Lynch, O. Chen, Z. Wang, X. Wang, D. LaMontagne, H. Wu, Z. Wang, Y. C. Cao, *Science* **2012**, *338*, 358.

[51] A. Castelli, J. De Graaf, S. Marras, R. Brescia, L. Goldoni, L. Manna, M. P. Arciniegas, *Nat. Commun.* **2018**, *9*, 1.

[52] K. Miszta, J. De Graaf, G. Bertoni, D. Dorfs, R. Brescia, S. Marras, L. Ceseracciu, R. Cingolani, R. Van Roij, M. Dijkstra, L. Manna, *Nat. Mater.* **2011**, *10*, 872.

[53] M. A. Boles, D. V. Talapin, *J. Am. Chem. Soc.* **2014**, *136*, 5868.

[54] I. Orue, L. Marcano, P. Bender, A. García-Prieto, S. Valencia, M. A. Mawass, D. Gil-Cartón, D. Alba Venero, D. Honecker, A. García-Arribas, L. Fernández Barquín, A. Muela, M. L. Fdez-Gubieda, *Nanoscale* **2018**, *10*, 7407.

[55] I. Morales, R. Costo, N. Mille, J. Carrey, A. Hernando, P. de la Presa, *Nanoscale Adv.* **2021**, *3*, 5801.

[56] D. Gandia, L. Gandarias, I. Rodrigo, J. Robles-García, R. Das, E. Garaio, J. Ángel García, M.-H. Phan, H. Srikanth, I. Orue, J. Alonso, A. Muela, M. Luisa Fdez-Gubieda, D. Gandia, I. Rodrigo, J. Á García, A. Muela, M. L. Fdez-Gubieda, L. Gandarias, J. Robles-García, R. Das, M. Phan, H. Srikanth, *Small* **2019**, *15*, 1902626.

[57] J. M. Asensio, J. Marbaix, N. Mille, L.-M. Lacroix, K. Soulantica, P.-F. Fazzini, J. Carrey, B. Chaudret, *Nanoscale* **2019**, *11*, 5402.

[58] J. Mohapatra, J. Elkins, M. Xing, D. Guragain, S. R. Mishra, J. P. Liu, *Nanoscale* **2021**, *13*, 4519.

[59] X. Zhang, L. Lv, L. Ji, G. Guo, L. Liu, D. Han, B. Wang, Y. Tu, J. Hu, D. Yang, A. Dong, *J. Am. Chem. Soc* **2016**, *138*, 3290.

[60] H. Wang, H. Zhang, C. Wu, B. Yang, Q. Zhang, B. Zhang, *RSC Adv* **2016**, *6*, 97882.

[61] G. Singh, H. Chan, A. Baskin, E. Gelman, N. Repnin, P. Král, R. Klajn, *Science* **2014**, *345*, 1149.

[62] M. Ma, Q. Zhang, J. Dou, H. Zhang, D. Yin, W. Geng, Y. Zhou, *J. Colloid. Interface. Sci* **2012**, *374*, 339.

[63] D. Liu, R. Aleisa, Z. Cai, Y. Li, Y. Yin, *Matter* **2021**, *4*, 927.

[64] E. Myrovali, K. Papadopoulos, I. Iglesias, M. Spasova, M. Farle, U. Wiedwald, M. Angelakeris, *ACS. Appl. Mater. Interfaces* **2021**, *13*, 21602.

[65] J. J. Brunner, M. Krumova, H. Cölfen, E. V. Sturm (née Rosseeva), *Beilstein. J. Nanotechnol.* **2019**, *10*, 894.

[66] N. C. Bigall, C. Wilhelm, M. L. Beoutis, M. García-Hernandez, A. A. Khan, C. Giannini, A. Sánchez-Ferrer, M. Mezzenga, M. E. Materia, M. A. Garcia, F. Gazeau, A. M. Bittner, L. Manna, T. Pellegrino, *Chem. Mater.* **2013**, *25*, 1055.

[67] N. C. Bigall, A. Curcio, M. P. Leal, A. Falqui, D. Palumberi, R. Di Corato, E. Albanesi, R. Cingolani, T. Pellegrino, *Adv. Mater.* **2011**, *23*, 5645.

[68] J. Xu, H. Zhang, Y. Zhang, X. Zhang, T. Wang, S. Hong, W. Wei, T. Zhao, W. Fang, *Nanoscale Res.* **2022**, *4*, 782.

[69] X. Ni, Q. Zhao, D. Zhang, X. Zhang, H. Zheng, *J. Phys. Chem. C* **2007**, *111*, 601.

[70] Y. Hou, H. Kondoh, T. Ohta, *Chem. Mater.* **2005**, *17*, 3994.

[71] J. Nai, B. Y. Guan, L. Yu, X. Wen, D. Lou, *Sci. Adv.* **2017**, *3*, 1700732.

[72] S. Sin gamaneni, V. N. Bliznyuk, C. Binek, E. Y. Tsymbal, *J. Mater. Chem.* **2011**, *21*, 16819.

[73] J. Gong, G. Li, Z. Tang, *Nano Today* **2012**, *7*, 564.

[74] A. Sánchez-Iglesias, N. Claes, D. M. Solís, J. M. Taboada, S. Bals, L. M. Liz-Marzán, M. Grzelczak, *Angew. Chem.* **2018**, *130*, 3237.

[75] A. Sánchez-Iglesias, M. Grzelczak, T. Altantzis, B. Goris, J. Pérez-Juste, S. Bals, G. Van Tendeloo, S. H. Donaldson, B. F. Chmelka, J. N. Israelachvili, L. M. Liz-Marzán, *ACS Nano* **2012**, *6*, 11059.

[76] M. Grzelczak, A. Sánchez-Iglesias, L. M. Liz-Marzán, *Soft Matter* **2013**, *9*, 9094.

[77] C. Kuttner, R. P. M. Höller, M. Quintanilla, M. J. Schnepf, M. Dulle, A. Fery, L. M. Liz-Marzán, *Nanoscale* **2019**, *11*, 17655.

[78] K. J. Si, D. Sikdar, Y. Chen, F. Eftekhari, Z. Xu, Y. Tang, W. Xiong, P. Guo, S. Zhang, Y. Lu, Q. Bao, W. Zhu, M. Premaratne, W. Cheng, *ACS Nano* **2014**, *8*, 11086.

[79] N. Li, M. Zhang, Y. Zha, Y. Cao, Y. Ma, *J. Colloid Interface. Sci.* **2020**, *575*, 54.

[80] X. Qiao, B. Su, C. Liu, Q. Song, D. Luo, G. Mo, T. Wang, X. Z. Qiao, C. Liu, Q. Song, D. Luo, T. Wang, B. S. Su, G. Mo, *Adv. Mater.* **2018**, *30*, 1702275.

[81] T. Kang, J. Zhu, X. Luo, W. Jia, P. Wu, C. Cai, *Anal. Chem.* **2021**, *93*, 2519.

[82] J. Li, W. Li, Y. Rao, F. Shi, S. Yu, H. Yang, L. Min, Z. Yang, *Chinese. Chem. Lett.* **2021**, *32*, 150.

[83] B. Tim, P. Błaszkiewicz, M. Kotkowiak, *Int. J. Mol. Sci.* **2022**, *23*, https://doi.org/10.3390/IJMS23010291.

[84] D. Grzelak, P. Szustakiewicz, C. Tollan, S. Raj, P. Král, W. Lewandowski, L. M. Liz-Marzán, *J. Am. Chem. Soc.* **2020**, *142*, 18814.

[85] G. A. Vinnacombe-Willson, Y. Conti, S. J. Jonas, P. S. Weiss, A. Mihi, L. Scarabelli, G. A. Vinnacombe-Willson, P. S. Weiss, Y. Conti, A. Mihi, L. Scarabelli, S. J. Jonas, *Adv. Mater.* **2022**, *34*, 2205330.

[86] B. Landeke-Wilsmark, L. Nyholm, C. Hägglund, *Langmuir* **2021**, *37*, 6032.

[87] S. Kim, C. Y. Zheng, G. C. Schatz, K. Aydin, K. H. Kim, C. A. Mirkin, *Nano Lett.* **2020**, *20*, 8096.

[88] J. Henzie, M. Grünwald, A. Widmer-Cooper, P. L. Geissler, P. Yang, *Nat. Mater.* **2011**, *11*, 131.

[89] Y. Wang, J. Chen, Y. Zhong, S. Jeong, R. Li, X. Ye, *J. Am. Chem. Soc.* **2022**, *144*, 13538.

[90] Z. Cheng, M. R. Jones, *Nat. Commun.* **2022**, *13*, 1.

[91] T. Paik, B. T. Diroll, C. R. Kagan, C. B. Murray, *J. Am. Chem. Soc.* **2015**, *137*, 6662.

[92] X. Ye, J. A. Millan, M. Engel, J. Chen, B. T. Diroll, S. C. Glotzer, C. B. Murray, *Nano Lett.* **2013**, *13*, 4988.

[93] E. V. Shevchenko, D. V. Talapin, C. B. Murray, S. O'Brien, *J. Am. Chem. Soc.* **2006**, *128*, 3620.

[94] E. V. Shevchenko, D. V. Talapin, N. A. Kotov, S. O'Brien, C. B. Murray, *Nature* **2006**, *439*, 55.

[95] T. Paik, C. B. Murray, *Nano. Lett.* **2013**, *13*, 2952.

[96] F. X. Redl, K. S. Cho, C. B. Murray, S. O'Brien, *Nature* **2003**, *423*, 968.

[97] I. Cherniukh, G. Rainò, T. Stöferle, M. Burian, A. Travesset, D. Naumenko, H. Amenitsch, R. Erni, R. F. Mahrt, M. I. Bodnarchuk, M. V. Kovalenko, *Nature* **2021**, *593*, 535.

[98] I. Cherniukh, T. V. Sekh, G. Rainò, O. J. Ashton, M. Burian, A. Travesset, M. Athanasiou, A. Manoli, R. A. John, M. Svyrydenko, V. Morad, Y. Shynkarenko, F. Montanarella, D. Naumenko, H. Amenitsch, G. Itskos, R. F. Mahrt, T. Stöferle, R. Erni, M. V. Kovalenko, M. I. Bodnarchuk, *ACS Nano* **2022**, *16*, 59.

[99] W. C. Zhang, M. D. Luoshan, P. F. Wang, C. Y. Huang, Q. Q. Wang, S. J. Ding, L. Zhou, *Nanomaterials* **2020**, *10*, 2207.

[100] A. La Porta, A. Sánchez-Iglesias, T. Altantzis, S. Bals, M. Grzelczak, L. M. Liz-Marzán, *Nanoscale* **2015**, *7*, 10377.

[101] B. Ni, G. Gonzalez-Rubio, H. Cölfen, *Acc. Chem. Res.* **2022**, *55*, 1599.

[102] C. Jenewein, J. Avaro, C. Appel, M. Liebi, H. Cölfen, *Angew. Chem. Int. Ed.* **2022**, *61*, 202112461.

[103] Z. Yin, Y. Zhou, P. Cui, J. Liao, M. H. Rafailovich, W. Sun, *Chem. Commun.* **2020**, *56*, 4808.

[104] O. Graniel, I. Iatsunskyi, E. Coy, C. Humbert, G. Barbillon, T. Michel, D. Maurin, S. Balme, P. Miele, M. Bechelany, *J. Mater. Chem. C. Mater.* **2019**, *7*, 15066.

[105] O. Graniel, I. Iatsunskyi, E. Coy, C. Humbert, G. Barbillon, T. Michel, D. Maurin, S. Balme, P. Miele, M. Bechelany, *J. Mater. Chem. C. Mater.* **2019**, *7*, 15066.

[106] S. Tang, Y. Li, H. Huang, P. Li, Z. Guo, Q. Luo, Z. Wang, P. K. Chu, J. Li, X. F. Yu, *ACS. Appl. Mater. Interfaces* **2017**, *9*, 7472.

[107] L. Chen, B. Su, L. Jiang, *Chem. Soc. Rev.* **2019**, *48*, 8.

[108] B. Cai, V. Sayevich, N. Gaponik, A. Eychmüller, B. Cai, V. Sayev, N. Gaponik, A. Eychmüller, *Adv. Mater.* **2018**, *30*, 1707518.

[109] M. Sainato, B. Shevitski, A. Sahu, J. D. Forster, S. Aloni, G. Barillaro, J. J. Urban, *ACS Omega* **2017**, *2*, 3681.

[110] J. A. Berrocal, G. H. Heideman, B. F. M. De Waal, M. Enache, R. W. A. Havenith, M. Stöhr, E. W. Meijer, B. L. Feringa, *J. Am. Chem. Soc.* **2020**, *142*, 4070.

[111] B. B. V. Salzmann, M. M. Van Der Sluijs, G. Soligno, D. Vanmaekelbergh, *Acc. Chem. Res.* **2021**, *54*, 787.

[112] P. Sutter, E. Sutter, *Acc. Chem. Res.* **2021**, *54*, 11.

[113] X. Li, Z. Xue, X. Chen, X. Qiao, G. Mo, W. Bu, B. Guan, T. Wang, *Sci. Adv.* **2022**, *8*, 1559.

[114] P. Tamarat, E. Prin, Y. Berezovska, A. Moskalenko, T. P. T. Nguyen, C. Xia, L. Hou, J. B. Trebbia, M. Zacharias, L. Pedesseau, C. Katan, M. I. Bodnarchuk, M. V. Kovalenko, J. Even, B. Lounis, *Nat. Commun.* **2023**, *14*, 1.

[115] A. Jana, A. Meena, S. A. Patil, Y. Jo, S. Cho, Y. Park, V. G. Sree, H. Kim, H. Im, R. A. Taylor, *Prog. Mater. Sci* **2022**, *129*, 100975.

[116] M. Sasaki, S. Hashimoto, Y. Iso, Y. Oaki, T. Isobe, H. Imai, *Nanoscale Adv.* **2023**, *5*, 2553.

[117] N. Hüsing, U. Schubert, *Angew. Chem. Int. Ed.* **1998**, *37*, 22.

[118] C. Ziegler, A. Wolf, W. Liu, A.-K. Herrmann, N. Gaponik, A. Eychmüller, *Angew. Chem. Int. Ed.* **2017**, *56*, 13200.

[119] N. Gaponik, A. K. Herrmann, A. Eychmüller, *J. Phys. Chem. Lett.* **2012**, *3*, 8.

[120] P. Rusch, D. Zámbó, N. C. Bigall, *Acc. Chem. Res* **2020**, *53*, 2414.

[121] F. Rechberger, M. Niederberger, *Nanoscale Horiz.* **2017**, *2*, 6.

[122] F. Matter, A. L. Luna, M. Niederberger, *Nano Today* **2019**, 100827.

[123] S. S. Kistler, *Nature* **1931**, *127*, 741.

[124] J. L. Mohanan, S. L. Brock, *J. Non. Cryst. Solids* **2004**, *350*, 1.

[125] T. Gacoin, L. Malier, J. P. Boilot, *Chem. Mater.* **1997**, *9*, 1502.

[126] J. L. Mohanan, I. U. Arachchige, S. L. Brock, *Science* **2005**, *307*, 397.

[127] S. Naskar, A. Freytag, J. Deutsch, N. Wendt, P. Behrens, A. Köckritz, N. C. Bigall, *Chem. Mater.* **2017**, *29*, 9208.

[128] S. Sánchez-Paradinas, D. Dorfs, S. Friebe, A. Freytag, A. Wolf, N. C. Bigall, *Adv. Mater.* **2015**, *27*, 6152.

[129] S. Naskar, J. F. Miethe, S. Sánchez-Paradinas, N. Schmidt, K. Kanthasamy, P. Behrens, H. Pfnür, N. C. Bigall, *Chem. Mater.* **2016**, *28*, 2089.

[130] N. Gaponik, A. Wolf, R. Marx, V. Lesnyak, K. Schilling, A. Eychmüller, *Adv. Mater.* **2008**, *20*, 4257.

[131] T. Hendel, V. Lesnyak, L. Kühn, A. Herrmann, N. C. Bigall, L. Borchardt, S. Kaskel, N. Gaponik, A. Eychmüller, *Adv. Funct. Mater.* **2013**, *23*, 1903.

[132] D. Zámbó, A. Schlosser, P. Rusch, F. Lübkemann, J. Koch, H. Pfnür, N. C. Bigall, *Small* **2020**, *16*, 1906934.

[133] V. Lesnyak, S. V. Voitekhovich, P. N. Gaponik, N. Gaponik, A. Eychmüller, *ACS Nano* **2010**, *4*, 4090.

[134] V. Lesnyak, A. Dubavik, L. Borchardt, S. V. Voitekhovich, N. Gaponik, S. Kaskel, A. Eychmüller, *J. Am. Chem. Soc.* **2011**, *133*, 13413.

[135] C. Rengers, S. V. Voitekhovich, S. Kittler, A. Wolf, M. Adam, N. Gaponik, S. Kaskelc, A. Eychmüller, *Nanoscale* **2015**, *7*, 12713.

[136] N. C. Bigall, A.-K. Herrmann, M. Vogel, M. Rose, P. Simon, W. Carrillo-Cabrera, D. Dorfs, S. Kaskel, N. Gaponik, A. Eychmüller, *Angew. Chem. Int. Ed.* **2009**, *48*, 9731.

[137] H. Chen, V. Lesnyak, N. C. Bigall, N. Gaponik, A. Eychmüller, *Chem. Mater.* **2010**, *22*, 2309.

[138] C. Ziegler, S. Klosz, L. Borchardt, M. Oschatz, S. Kaskel, M. Friedrich, R. Kriegel, T. Keilhauer, M. Armbrüster, A. Eychmüller, *Adv. Funct. Mater* **2016**, *26*, 1014.

[139] A. Schlosser, L. C. Meyer, F. Lübkemann, J. F. Miethe, N. C. Bigall, *Phys. Chem. Chem. Phys.* **2019**, *21*, 9002.

[140] D. Zámbó, P. Rusch, F. Lübkemann, N. C. Bigall, *ACS. Appl. Mater. Interfaces* **2021**, *13*, 57774.

[141] A. Freytag, S. Sánchez-Paradinas, S. Naskar, N. Wendt, M. Colombo, G. Pugliese, J. Poppe, C. Demirci, I. Kretschmer, D. W. Bahnemann, P. Behrens, N. C. Bigall, *Angew. Chem. Int. Ed.* **2016**, *55*, 1200.

[142] I. U. Arachchige, J. L. Mohanan, S. L. Brock, *Chem. Mater.* **2005**, *17*, 6644.

[143] J. Schlenkrich, D. Zámbó, A. Schlosser, P. Rusch, N. C. Bigall, *Adv. Opt. Mater.* **2022**, *10*, https://doi.org/10.1002/adom.202101712.

[144] N. Leventis, N. Chandrasekaran, C. Sotiriou-Leventis, A. Mumtaz, *J. Mater. Chem.* **2009**, *19*, 63.

[145] M. A. Hettiarachchi, T. Su'A, A. H. Ramzan, S. Pokhrel, B. Nadgorny, S. L. Brock, *J. Phys. Chem. C* **2022**, *126*, 2088.

[146] A. Freytag, C. Günnemann, S. Naskar, S. Hamid, F. Lübkemann, D. Bahnemann, N. C. Bigall, *ACS Appl. Nano. Mater* **2018**, *1*, 6123.

[147] M. Rosebrock, D. Zámbó, P. Rusch, D. Pluta, F. Steinbach, P. Bessel, A. Schlosser, A. Feldhoff, K. D. J. Hindricks, P. Behrens, D. Dorfs, N. C. Bigall, *Adv. Funct. Mater.* **2021**, *31*, 2170301.

[148] G. Jiang, J. Wang, N. Li, R. Hübner, M. Georgi, B. Cai, Z. Li, V. Lesnyak, N. Gaponik, A. Eychmüller, *Chem. Mater.* **2022**, *34*, 2696.

[149] L. Korala, J. R. Germain, E. Chen, I. R. Pala, D. Li, S. L. Brock, *Inorg. Chem. Front.* **2017**, *4*, 1451.

[150] F. J. Heiligtag, W. Cheng, V. R. De Mendonça, M. J. Süess, K. Hametner, D. Günther, C. Ribeiro, M. Niederberger, *Chem. Mater.* **2014**, *26*, 5576.

[151] W. Wan, R. Zhang, M. Ma, Y. Zhou, *J. Mater. Chem. A. Mater* **2018**, *6*, 754.

[152] B. Cai, D. Wen, W. Liu, A. K. Herrmann, A. Benad, A. Eychmüller, *Angew. Chem. Int. Ed.* **2015**, *54*, 13101.

[153] W. Liu, A. K. Herrmann, N. C. Bigall, P. Rodriguez, D. Wen, M. Oezaslan, T. J. Schmidt, N. Gaponik, A. Eychmüller, *Acc. Chem. Res* **2015**, *48*, 154.

[154] D. Müller, D. Zámbó, D. Dorfs, N. C. Bigall, *Small* **2021**, *17*, 2007908.

[155] Q. Yao, S. L. Brock, *Nanotechnology* **2010**, *21*, 115502.

[156] S. Ganguly, C. Zhou, D. Morelli, J. Sakamoto, S. L. Brock, *J. Phys. Chem. C* **2012**, *116*, 17431.

[157] T. Gacoin, L. Malier, J.-P. Boilot, *J. Mater. Chem.* **1997**, *7*, 859.

[158] V. Sayevich, B. Cai, A. Benad, D. Haubold, L. Sonntag, N. Gaponik, V. Lesnyak, A. Eychmüller, *Angew. Chem. Int. Ed.* **2016**, *55*, 6334.

[159] N. Gaponik, A. Wolf, R. Marx, V. Lesnyak, K. Schilling, A. Eychmüller, *Adv. Mater.* **2008**, *20*, 4257.

[160] S. Ganguly, S. L. Brock, *J. Mater. Chem.* **2011**, *21*, 8800.

[161] I. R. Pala, S. L. Brock, *ACS. Appl. Mater. Interfaces* **2012**, *4*, 2160.

[162] I. U. Arachchige, S. L. Brock, *J. Am. Chem. Soc.* **2007**, *129*, 1840.

[163] P. Rusch, D. Pluta, F. Lübkemann, D. Dorfs, D. Zámbó, N. C. Bigall, *Chem. Phys. Chem.* **2022**, *23*, https://doi.org/10.1002/cphc.202100755.

[164] A. Schlosser, L. C. Meyer, F. Lübkemann, J. F. Miethe, N. C. Bigall, *Phys. Chem. Chem. Phys.* **2019**, *21*, 9002.

[165] L. Carbone, C. Nobile, M. De Giorgi, F. Della Sala, G. Morello, P. Pompa, M. Hytch, E. Snoeck, A. Fiore, I. R. Franchini, M. Nadasan, A. F. Silvestre, L. Chiodo, S. Kudera, R. Cingolani, R. Krahne, L. Manna, *Nano Lett.* **2007**, *7*, 2942.

[166] P. Rusch, B. Schremmer, C. Strelow, A. Mews, D. Dorfs, N. C. Bigall, *J. Phys. Chem. Lett.* **2019**, *10*, 7804.

[167] F. Lübkemann, J. F. Miethe, F. Steinbach, P. Rusch, A. Schlosser, D. Zámbó, T. Heinemeyer, D. Natke, D. Zok, D. Dorfs, N. C. Bigall, *Small* **2019**, *15*, 1902186.

[168] J. F. Miethe, F. Luebkemann, A. Schlosser, D. Dorfs, N. C. Bigall, *Langmuir* **2020**, *36*, 4757.

[169] L. Korala, J. R. Germain, E. Chen, I. R. Pala, D. Li, S. L. Brock, *Inorg. Chem. Front* **2017**, *4*, 1451.

[170] J. Schlenkrich, F. Lübkemann-Warwas, R. T. Graf, C. Wesemann, L. Schoske, M. Rosebrock, K. D. J. Hindricks, P. Behrens, D. W. Bahnemann, D. Dorfs, N. C. Bigall, *Small* **2023**, 2208108.

[171] G. Jiang, J. Wang, N. Li, R. Hübner, M. Georgi, B. Cai, Z. Li, V. Lesnyak, N. Gaponik, A. Eychmüller, *Chem. Mater.* **2022**, *34*, 2687.

[172] M. A. Hettiarachchi, T. Su'A, A. H. Ramzan, S. Pokhrel, B. Nadgorny, S. L. Brock, *J. Phys. Chem. C* **2022**, *126*, 2088.

[173] F. J. Heiligtag, M. J. I. Airaghi Leccardi, D. Erdem, M. J. Süess, M. Niederberger, *Nanoscale* **2014**, *6*, 13213.

[174] H. Maleki, L. Durães, B. F. O. Costa, R. F. Santos, A. Portugal, *Microporous. Mesoporous Mater.* **2016**, *232*, 227.

[175] L. Amirkhani, J. Moghaddas, H. Jafarizadeh-Malmiri, *RSC Adv.* **2016**, *6*, 12676.

[176] Z. S. Wu, S. Yang, Y. Sun, K. Parvez, X. Feng, K. Müllen, *J. Am. Chem. Soc.* **2012**, *134*, 9082.

[177] X. Xu, H. Li, Q. Zhang, H. Hu, Z. Zhao, J. Li, J. Li, Y. Qiao, Y. Gogotsi, *ACS Nano* **2015**, *9*, 3969.

[178] M. Helminger, B. Wu, T. Kollmann, D. Benke, D. Schwahn, V. Pipich, D. Faivre, D. Zahn, H. Cölfen, *Adv. Funct. Mater.* **2014**, *24*, 3187.

[179] S. Sturm, M. Siglreitmeier, D. Wolf, K. Vogel, M. Gratz, D. Faivre, A. Lubk, B. Büchner, E. V. Sturm, H. Cölfen, *Adv. Funct. Mater.* **2019**, *29*, https://doi.org/10.1002/ADFM.201905996.

[180] L. Altenschmidt, S. Sánchez-Paradinas, F. Lübkemann, D. Zámbó, A. M. Abdelmonem, H. Bradtmüller, A. Masood, I. Morales, P. de la Presa, A. Knebel, M. A. G. García-Tuñón, B. Pelaz, K. D. J. Hindricks, P. Behrens, W. J. Parak, N. C. Bigall, *ACS. Appl. Nano. Mater.* **2021**, *4*, 6678.

[181] N. Shah, T. Rehan, X. Li, H. Tetik, G. Yang, K. Zhao, D. Lin, *RSC. Adv.* **2021**, *11*, 7187.

[182] N. C. Bigall, A.-K. Herrmann, M. Vogel, M. Rose, P. Simon, W. Carrillo-Cabrera, D. Dorfs, S. Kaskel, N. Gaponik, A. Eychmüller, *Angew. Chem. Int. Ed.* **2009**, *48*, 9731.

[183] W. Liu, A. K. Herrmann, D. Geiger, L. Borchardt, F. Simon, S. Kaskel, N. Gaponik, A. Eychmüller, *Angew. Chem. Int. Ed.* **2012**, *51*, 5743.

[184] W. Liu, P. Rodriguez, L. Borchardt, A. Foelske, J. Yuan, A. K. Herrmann, D. Geiger, Z. Zheng, S. Kaskel, N. Gaponik, R. Kötz, T. J. Schmidt, A. Eychmüller, *Angew. Chem. Int. Ed.* **2013**, *52*, 9849.

[185] C. Zhu, D. Wen, M. Oschatz, M. Holzschuh, W. Liu, A. K. Herrmann, F. Simon, S. Kaskel, A. Eychmüller, *Small* **2015**, *11*, 1430.

[186] W. Liu, A. K. Herrmann, N. C. Bigall, P. Rodriguez, D. Wen, M. Oezaslan, T. J. Schmidt, N. Gaponik, A. Eychmüller, *Acc. Chem. Res.* **2015**, *48*, 154.

[187] D. Wen, W. Liu, D. Haubold, C. Zhu, M. Oschatz, M. Holzschuh, A. Wolf, F. Simon, S. Kaskel, A. Eychmüller, *ACS Nano* **2016**, *10*, 2559.

[188] A. Freytag, M. Colombo, N. C. Bigall, *Z. Phys. Chem.* **2017**, *231*, 63.

[189] R. Du, W. Jin, H. Wu, R. Hübner, L. Zhou, G. Xue, Y. Hu, A. Eychmüller, *J. Mater. Chem. A Mater.* **2021**, *9*, 17189.

[190] R. Du, J. O. Joswig, R. Hübner, L. Zhou, W. Wei, Y. Hu, A. Eychmüller, *Angew. Chem. Int. Ed.* **2020**, *59*, 8293.

[191] J. S. Diercks, M. Georgi, J. Herranz, N. Diklić, P. Chauhan, A. H. Clark, R. Hübner, A. Faisnel, Q. Chen, M. Nachtegaal, A. Eychmüller, T. J. Schmidt, *ACS. Appl. Energy Mater.* **2022**, *5*, 8460.

[192] B. Cai, D. Wen, W. Liu, A.-K. Herrmann, A. Benad, A. Eychmüller, *Angew. Chem.* **2015**, *127*, 13293.

[193] S. Henning, L. Kühn, J. Herranz, J. Durst, T. Binninger, M. Nachtegaal, M. Werheid, W. Liu, M. Adam, S. Kaskel, A. Eychmüller, T. J. Schmidt, *J. Electrochem. Soc.* **2016**, *163*, F998.

[194] P. Khavlyuk, A. Mitrofanov, V. Shamraienko, R. Hübner, J. Kresse, K. B. L. Borchert, A. Eychmüller, *Chem. Mater.* **2023**, *35*, 2864.

[195] P. Chauhan, K. Hiekel, J. S. Diercks, J. Herranz, V. A. Saveleva, P. Khavlyuk, A. Eychmüller, T. J. Schmidt, *ACS. Mater. Au* **2021**, *2*, 278.

[196] D. Müller, L. F. Klepzig, A. Schlosser, D. Dorfs, N. C. Bigall, *Langmuir* **2021**, *37*, 5109.

[197] D. Zámbó, P. Rusch, F. Lü, N. C. Bigall, *ACS Appl. Mater. Interfaces* **2021**, *13*, 57785.

[198] A. Freytag, C. Günnemann, S. Naskar, S. Hamid, F. Lübkemann, D. Bahnemann, N. C. Bigall, *ACS. Appl. Nano. Mater* **2018**, *1*, 6123.

[199] J. Schlenkrich, D. Zámbó, A. Schlosser, P. Rusch, N. C. Bigall, *Adv. Opt. Mater* **2022**, *10*, 2101712.

[200] V. Lesnyak, A. Wolf, A. Dubavik, L. Borchardt, S. V. Voitekhovich, N. Gaponik, S. Kaskel, A. Eychmüller, *J. Am. Chem. Soc.* **2011**, *133*, 13413.

[201] T. Hendel, V. Lesnyak, L. Kühn, A.-K. Herrmann, N. C. Bigall, L. Borchardt, S. Kaskel, N. Gaponik, A. Eychmüller, *Adv. Funct. Mater.* **2013**, *23*, 1903.

[202] S. K. Gill, L. J. Hope-Weeks, *Chem. Commun.* **2009**, 4384.

[203] A. Schlosser, J. Schlenkrich, D. Zámbó, M. Rosebrock, R. T. Graf, E. Cano, N. C. Bigall, **2022**, *9*, 2200055.

[204] P. Rusch, F. Niemeyer, D. Pluta, B. Schremmer, F. Lübkemann, M. Rosebrock, M. Schäfer, M. Jahns, P. Behrens, N. C. Bigall, *Nanoscale* **2019**, *11*, 15270.

[205] F. J. Heiligtag, M. D. Rossell, M. J. Süess, M. Niederberger, *J. Mater. Chem.* **2011**, *21*, 16893.

[206] F. Rechberger, M. Niederberger, *Mater. Horiz.* **2017**, *4*, 1115.

[207] J. Kwon, K. Choi, E. Tervoort, M. Niederberger, *J. Mater. Chem. A* **2022**, *10*, 18383.

[208] M. R. Hoffmann, S. T. Martin, W. Choi, D. W. Bahnemann, *Chem. Rev.* **1995**, *95*, 69.

[209] J. Schneider, D. W. Bahnemann, *J. Phys. Chem. Lett.* **2013**, *4*, 3479.

[210] V. Etacheri, C. Di Valentin, J. Schneider, D. Bahnemann, S. C. Pillai, *J. Photochem. Photobiol. C Photochem. Rev.* **2015**, *25*, 1.

[211] P. Kalisman, Y. Nakibli, L. Amirav, *Nano Lett.* **2016**, *16*, 1776.

[212] Y. Nakibli, Y. Mazal, Y. Dubi, M. Wächtler, L. Amirav, *Nano. Lett.* **2018**, *18*, 357.

[213] F. Lübkemann, J. Frederick Miethe, F. Steinbach, P. Rusch, A. Schlosser, D. Zámbó, T. Heinemeyer, D. Natke, D. Zok, D. Dorfs, N. C. Bigall, F. Lübkemann, J. F. Miethe, F. Steinbach, P. Rusch, A. Schlosser, D. Zámbó, T. Heinemeyer, D. Natke, D. Zok, D. Dorfs, N. C. Bigall, *Small* **2019**, *15*, 1902186.

[214] K. Hiekel, S. Jungblut, M. Georgi, A. Eychmüller, *Angewa. Chem.* **2020**, *132*, 12146.

[215] P. Rusch, F. Niemeyer, D. Pluta, B. Schremmer, F. Lübkemann, M. Rosebrock, M. Schäfer, M. Jahns, P. Behrens, N. C. Bigall, *Nanoscale* **2019**, *11*, 15270.

[216] B. Cai, R. Hübner, K. Sasaki, Y. Zhang, D. Su, C. Ziegler, M. B. Vukmirovic, B. Rellinghaus, R. R. Adzic, A. Eychmüller, *Angew. Chem. Int. Ed.* **2018**, *57*, 2963.

[217] X. Zhang, L. Lv, L. Ji, G. Guo, L. Liu, D. Han, B. Wang, Y. Tu, J. Hu, D. Yang, A. Dong, *J. Am. Chem. Soc* **2016**, *138*, 3290.

[218] H. Wang, H. Zhang, C. Wu, B. Yang, Q. Zhang, B. Zhang, *RSC Adv* **2016**, *6*, 97882.

[219] S. Naskar, J. F. Miethe, S. Sánchez-Paradinas, N. Schmidt, K. Kanthasamy, P. Behrens, H. Pfnür, N. C. Bigall, *Chem. Mater.* **2016**, *28*, 2089.

[220] D. Zámbó, A. Schlosser, P. Rusch, F. Lübkemann, J. Koch, H. Pfnür, N. C. Bigall, *Small* **2020**, *16*, 1906934.

[221] A. Schlosser, L. C. Meyer, F. Lübkemann, J. F. Miethe, N. C. Bigall, *Phys. Chem. Chem. Phys.* **2019**, *21*, 9002.

[222] S. Sánchez-Paradinas, D. Dorfs, S. Friebe, A. Freytag, A. Wolf, N. C. Bigall, *Adv. Mater.* **2015**, *27*, 6152.

[223] P. Rusch, B. Schremmer, C. Strelow, A. Mews, D. Dorfs, N. C. Bigall, *J. Phys. Chem. Lett.* **2019**, *10*, 7804.

[224] P. Rusch, D. Pluta, F. Lübkemann, D. Dorfs, D. Zámbó, N. C. Bigall, *Chem. Phys. Chem.* **2022**, *23*, https://doi.org/10.1002/cphc.202100755.

[225] F. Lübkemann, J. F. Miethe, F. Steinbach, P. Rusch, A. Schlosser, D. Zámbó, T. Heinemeyer, D. Natke, D. Zok, D. Dorfs, N. C. Bigall, *Small* **2019**, *15*, 1902186.

[226] J. S. Diercks, M. Georgi, J. Herranz, N. Diklić, P. Chauhan, A. H. Clark, R. Hübner, A. Faisnel, Q. Chen, M. Nachtegaal, A. Eychmüller, T. J. Schmidt, *ACS. Appl. Energy Mater* **2022**, *5*, 8460.

[227] M. Rosebrock, D. Zámbó, P. Rusch, R. T. Graf, D. Pluta, H. Borg, D. Dorfs, N. C. Bigall, M. Rosebrock, P. Rusch, R. T. Graf, D. Pluta, H. Borg, D. Dorfs, N. C. Bigall, D. Zámbó, *Small* **2023**, *19*, 2206818.

**ADVANCED
SCIENCE NEWS**

www.advancedsciencenews.com

**small
structures**

www.small-structures.com

Franziska Lübkemann-Warwas was born in Sulingen in 1988. She received a B.Sc. in Chemistry and a M.Sc. in Material and Nanochemistry from Leibniz Universität Hannover in 2012 and 2015, respectively, followed by a doctorate in physical chemistry in the group of Prof. Bigall in 2020. Currently, she is a postdoctoral researcher in the group of Prof. Bigall. Her research interests cover the synthesis, characterization, and patterning of nanocrystal-based assemblies as well as their application in fields like photocatalysis.

Irene Morales was born in Madrid in 1991. She got her B.Sc. in Physics in 2015 and M.Sc. in Nanophysics and Advanced Materials in 2016 from the University Complutense of Madrid. She obtained her doctorate in Physics at the Institute of Applied Magnetism of the University Complutense of Madrid in 2021. Nowadays, she is a postdoctoral researcher in the group of Prof. Bigall at Leibniz Universität Hannover. Her research interests include the synthesis, characterization, and applications of multifunctional magnetic nanocrystal assemblies, in particular for magnetic hyperthermia, catalysis, and drug delivery.

Nadja C. Bigall was born in Munich in 1979. She graduated in physics at Ludwig Maximilians Universität in 2005, followed by a doctorate at TU Dresden in 2009 in physical chemistry. After postdoctoral work at the Italian Institute of Technology and at Philipps–Universität Marburg, she built up her research group at Leibniz Universität Hannover, where she became an associate professor in 2017 and full professor in 2018. Her research interests are the synthesis, characterization, and structure–property correlation of functional nanostructures, such as colloidal nanocrystals and assemblies thereof.